Hindawi Publishing Corporation
Journal of Sensors
Volume 2015, Article ID 548506, 25 pages
http://dx.doi.org/10.1155/2015/548506

Research Article

Monitoring of Damage in Sunflower and Maize Parcels Using Radar and Optical Time Series Data

György Surek and Gizella Nádor

Institute of Geodesy, Cartography and Remote Sensing, Bosnyák tér 5, Budapest 1149, Hungary

Correspondence should be addressed to Gizella Nádor; nador.gizella@fomi.hu

Received 26 December 2014; Accepted 24 April 2015

Academic Editor: Jian Yang

The objective of this paper is to monitor the temporal behaviour of geometrical structural change of cropland affected by four different types of damage: weed infection, Western Corn Rootworm (WCR), storm damage, and drought by time series of different type of optical and quad-pol RADARSAT2 data. Based on our results it is established that ragweed infection in sunflower can be well identified by evaluation of radar (mid-June) and optical (mid-August) satellite images. Effect of drought in sunflower is well recognizable by spectral indices derived from optical as well as "I"-component of Shannon entropy (SE_I) from radar satellite images acquired during the first decade of July. Evaluation of radar and optical satellite images acquired between the last decade of July and mid-August proven to be the most efficient for detecting damages in maize fields caused by either by WCR or storm. Components of Shannon entropy are proven to have significant role in identification. Our project demonstrates the potential in integrated usage of polarimetric radar and optical satellite images for monitoring several types of agricultural damage.

1. Introduction

Polarimetric characteristics of various crop types have been studied by a number of authors [1–3]. According to them these features depend on numerous properties of the reflecting surface element (e.g., surface reflectivity, water content, and roughness) particularly on the geometric structure of plants. Consequently, the polarimetric features can be applied for assessment of crop condition, identification of crop types, and phenological phases of crops [4–7]. This paper presents how damage may modify a plant's response to polarimetric radar beam. The objective is to determine whether optical and SAR time series can detect damage-induced spatial and temporal changes in crop structure.

Damage induces changes in spectral and geometric features of croplands. Therefore, the most efficient way of identification of this damage can be to coevaluate optical and polarimetric radar satellite images. Previous results of our survey on this subject have already been presented on several publications [8–10].

The objective of our investigation (presented in this paper) was to monitor the temporal structural changes of cropland affected by weed infection, WCR, and storm damage as well as drought in some study areas in Hungary by the integrated use of time series of optical and radar data. The temporal behaviour of 4 different types of damage has been surveyed, carried out on 3 distinct sample areas (Csongrád, Békés, and Baranya).

Effects of weed infection in sunflower had been examined over Baranya site. Weed infection generates discontinuities in regular geometry of row-sown crop cultivars. Figure 1 presents the difference between geometric structure of weed-infected and healthy sunflower parcels.

For Csongrád site drought-caused geometric changes in sunflower parcels had been examined and set against healthy sunflower fields. Figure 2 illustrates the differences in geometric structure of these two states in sunflower parcels.

As for Békés site, we examined two different types of damage occurring in corn fields, assessed in 2 different dates. Larvae of Western Corn Rootworm (WCR) attack the root

Figure 1: Demonstration of the difference between the geometric structure of ragweed infected and control (weed-free) sunflower fields.

Figure 2: Demonstration of the difference between geometric structure of control and drought stressed sunflower fields.

Figure 3: Geometric structure of WCR/storm damaged corn fields compared to the healthy ones (control) corn fields.

of the plant, which engender individual corn stems tumble; hence the parcel shows a rather bruised scenery. Figure 3 illustrates the scenic difference between the geometric structure of the damaged corn field and control one. Heavy storms may have similar effects on corn, although in that case stems lean according to wind direction. In both cases, geometric structure of corn field suffers appreciable changes, showing considerable differences compared to control parcels on which corn stems standing up orderly.

This paper presents the results of coevaluation of multitemporal RADARSAT-2 (standard quad-pol) and optical satellite images regarding to the abovementioned damage.

2. Materials and Methods

This paragraph presents the study areas selected, the data used (satellite and reference data), and methodology applied.

2.1. Study Areas. Our survey was applied to three distinct study areas: Csongrád, Baranya, and Békés sites (Figure 4).

Csongrád site, located between the river Tisza and the Danube, can be characterized by small-size parcels (its average parcel size is 1–5 hectares), sandy soils with poor water holding capacity; therefore the area is extremely sensitive to drought.

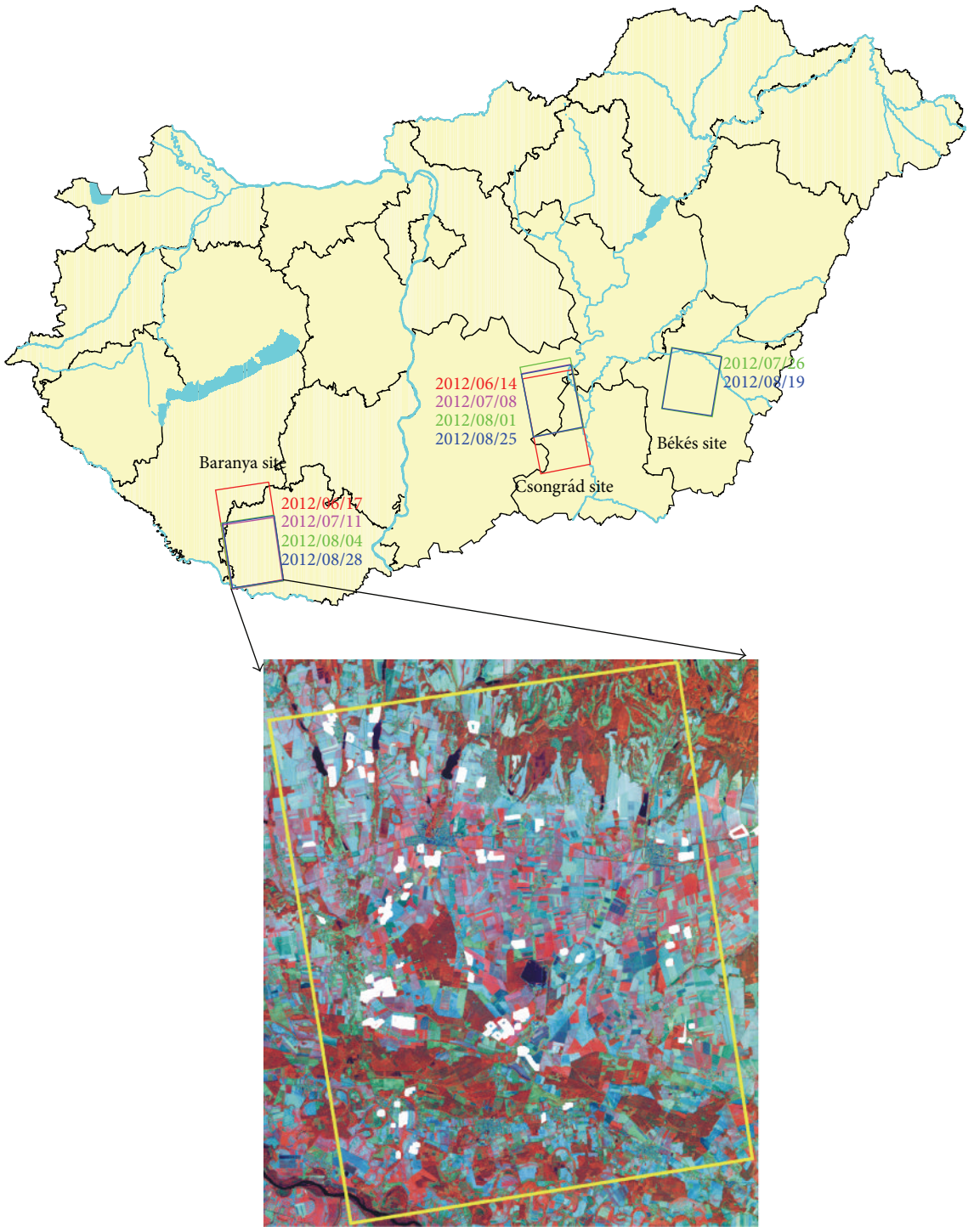

Figure 4: The location of the study areas and coverage of radar satellite images and location of reference parcels for Baranya site on SPOT5 (20/08/2012, R: NIR, G: SWIR, B: Red) satellite image composite.

Baranya site, located on the southern part of Transdanubia, has medium-size parcels (20–30 hectares). The area, sunflower in particular, is extremely infected by ragweed and numerous other types of weeds.

Békés site is located in the south-eastern part of the Hungarian Great Plain. Its average parcel-size takes 40–50 hectares. As being one of the most important corn-producing areas with maize monoculture, it opens the door to the spreading of WCR. The area was hit by serious storms several times in 2012. We analyzed the effects of storm which occurred on July 7, 2012.

2.2. Data Used. Coverage of satellite images and position of sample areas are presented on Figure 4.

Table 1: Data applied for Csongrád site.

Acquisition date RADARSAT2	Date of field survey	Optical satellite images and acquisition date
14/6/2012	14-15/06/2012	Landsat TM7 18/06/2012
8/7/2012	3–5/07/2012	Landsat TM7 04/07/2012, Geoeye: 30/06/2012, IRS-R2 AWiFS: 03/07/2012
1/8/2012	—	Landsat TM7 20/07/2012, SPOT5 29/07/2012, Landsat TM7 05/08/2012
25/8/2012	26/09/2012	SPOT5 19/08/2012, Landsat TM7 21/08/2012

Table 2: Data applied for Baranya site.

Acquisition date of RADARSAT2	Date of field survey	Optical satellite images and acquisition date
17/6/2012	17/6/2012	IRS-R2 LISS III 1/5/2012 Landsat TM7 31/5/2012 Landsat TM7 16/6/2012
11/7/2012	3-4/7/2012	IRS-P6 LISS III: 30/6/2012, Landsat TM7 02/7/2012, Landsat TM7 11/7/2012
4/8/2012	—	SPOT4: 28/7/2012, Landsat TM7 3/8/2012, IRS-R2 LISS III 5/8/2012
28/8/2012	24–26/9/2012	Landsat TM7 19/08/2012, SPOT5 20/08/2012, Landsat TM7 28/08/2012, IRS-P6 LISS III 10/09/2012

Table 3: Data applied for Békés site.

Acquisition date of RADARSAT2	Date of field survey	Optical satellite images and acquisition data
26/7/2012	6–8/8/2012	Landsat TM7 13/7/2012, Landsat TM7 20/7/2012, SPOT4 29/7/2012, IRS-P6 LISS III 8/8/2012
19/8/2012	—	Landsat TM7 14/8/2012, SPOT5 19/8/2012, Landsat TM7 30/8/2012

Features of the applied optical and radar satellite images (acquisition data, date of ground reference data collection, and other characteristics) are shown in Tables 1–3. Tables 4–9 contain the characterisation of the optical radar satellite images applied for the examinations. Each of the radar satellite images is coupled with optical satellite images acquired nearly at the same time. Although we tried our best, we did not always succeed in collecting ground reference data at the same time.

Reference data was collected from weed-infected sunflower parcels, WCR and storm damaged maize parcels, and sunflower parcels hit by drought. Control data was collected from correspondent healthy parcels as well. Results of reference data collecting are given in Tables 10–12.

Table 4: Characterisation of optical satellite images applied for Csongrád site.

Acquisition date	Satellite	Spatial resolution (m)	Spectral resolution
29/04/2012	IRS-P6 LISS III	20	Green, red, NIR, SWIR
01/05/2012	Landsat TM7	30	Blue, green, red, NIR, SWIR1, SWIR2
11/05/2012	IRS-R2 AWiFS	50	Green, red, NIR, SWIR
18/06/2012	Landsat TM7	30	Blue, green, red, NIR, SWIR1, SWIR2
30/06/2012	GEOEYE	0.5	Blue, green, red, NIR
01/07/2012	IRS-P6 AWiFS	50	Green, red, NIR, SWIR
03/07/2012	IRS-R2 AWiFS	50	Green, red, NIR, SWIR
04/07/2012	Landsat TM7	30	Blue, green, red, NIR, SWIR1, SWIR2
20/07/2012	Landsat TM7	30	Blue, green, red, NIR, SWIR1, SWIR2
29/07/2012	SPOT5	10	Green, red, NIR, SWIR
05/08/2012	Landsat TM7	30	Blue, green, red, NIR, SWIR1, SWIR2
05/08/2012	IRS-R2 AWiFS	50	Blue, green, red, NIR, SWIR1, SWIR2
19/08/2012	SPOT5	10	Green, red, NIR, SWIR
21/08/2012	Landsat TM7	30	Blue, green, red, NIR, SWIR1, SWIR2
06/10/2012	IRS-R2 AWiFS	50	Green, red, NIR, SWIR

2.3. Presentation of the Damages Examined. This paragraph describes the main effects of the various damage impacts. On Figures 5–7 we used special band combinations for colour composite to emphasize the difference between damaged and control areas.

2.3.1. Sunflower Hit by Drought. Figure 5 represents a typical sunflower parcel hit by drought (delineated by brown) contrarily to a healthy one (delineated by green) visualized on optical satellite image composite (Geoeye 30/6/2012, R: NIR, G: red, B: blue) and on radar data composite (RADARSAT2 8/7/2012, R: SE, G: SE_i, B: l3) as well.

Difference between the sunflower parcels can be well discernible on photos taken on the spot. As sunflowers hit by drought have sagging leaves, they cannot cover the soil completely, whilst leaves of healthy sunflower are horizontal and cover the entire soil surface.

Difference can be well identified on both optical and radar satellite composites. Healthy sunflower parcel appears orange on optical images, unlike those hit by drought showing bluish tinge which is typical to bare soil.

Table 5: Characterisation of radar satellite images applied for Csongrád site.

Acquisition date	Satellite	Spatial resolution (m)	Polarisation	Wavelength (cm)	Incidence angle (°)	Beam	Pass
14/06/2012	RADARSAT2	20	Quad-pol	5.6	37.4–38.9	SQ18	Ascending
08/07/2012	RADARSAT2	20	Quad-pol	5.6	37.4–38.9	SQ18	Ascending
01/08/2012	RADARSAT2	20	Quad-pol	5.6	37.4–38.9	SQ18	Ascending
25/08/2012	RADARSAT2	20	Quad-pol	5.6	37.4–38.9	SQ18	Ascending

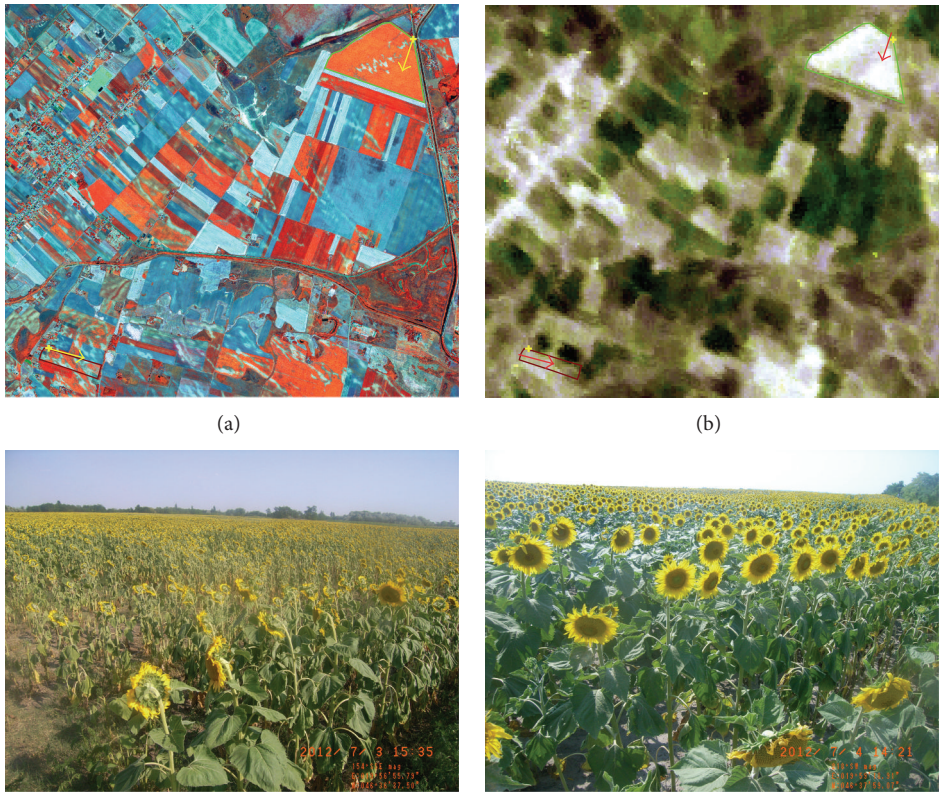

Figure 5: Sunflower hit by drought (marked by brown polygon) and control (marked by green polygon) sunflower fields on Geoeye (30/6/2012, R: NIR, G: red, B: blue) (a) and RADARSAT2 (8/7/2012, R: SE, G: SE_i, B: l3) satellite image composites (b) and photos taken on ground survey (3–5/07/2012) (c, d): sunflower hit by drought (c), control sunflower (d). Direction of the photos taken is shown by arrows.

On radar images appearance of healthy sunflower can be described with intense light colors, whilst damaged parcels are greenish-gray.

2.3.2. Appearance of Weed Infection in Sunflower Parcels. Figure 6 represents a typical sunflower parcel infected by weed (delineated by brown colour) contrarily to a control, weed-free one (delineated by green) visualized on optical satellite image composite (IRS-P6 LISS 30/6/2012, R: NIR, G: red, B: blue) and on radar data composite (RADARSAT2 17/06/2012, R: YAM_{odd}, G: SE, B: l2) as well, accompanied by photos taken on the spot on July 3 and 4, 2012.

Difference between these two sunflower parcels can be well discernible on photos. As weed-infected sunflower is less developed, weed and soil are usually revealed between the rows of plants, while leaves of healthy sunflower stand horizontal, covering the soil surface fully, making it invisible from above.

Difference can be well identified on radar satellite composite (17/6/2012), while it cannot be observed on the optical scene acquired on June 30, 2012.

2.3.3. WCR and Storm Damage in Maize Parcels. A typical maize parcel attacked by Western Corn Rootworm (delineated by brown colour) and another damaged by storm (delineated by blue), contrarily to a healthy one (delineated by green) are visualized on optical satellite image composites (a; SPOT4 29/06/2012, R: NIR, G: SWIR, B: red) (b; SPOT5 19/08/2012, R: NIR, G: SWIR, B: red), on radar data composites RADARSAT2 (26/07/2012, 19/08/2012, R: SE_p, G: SE_i,

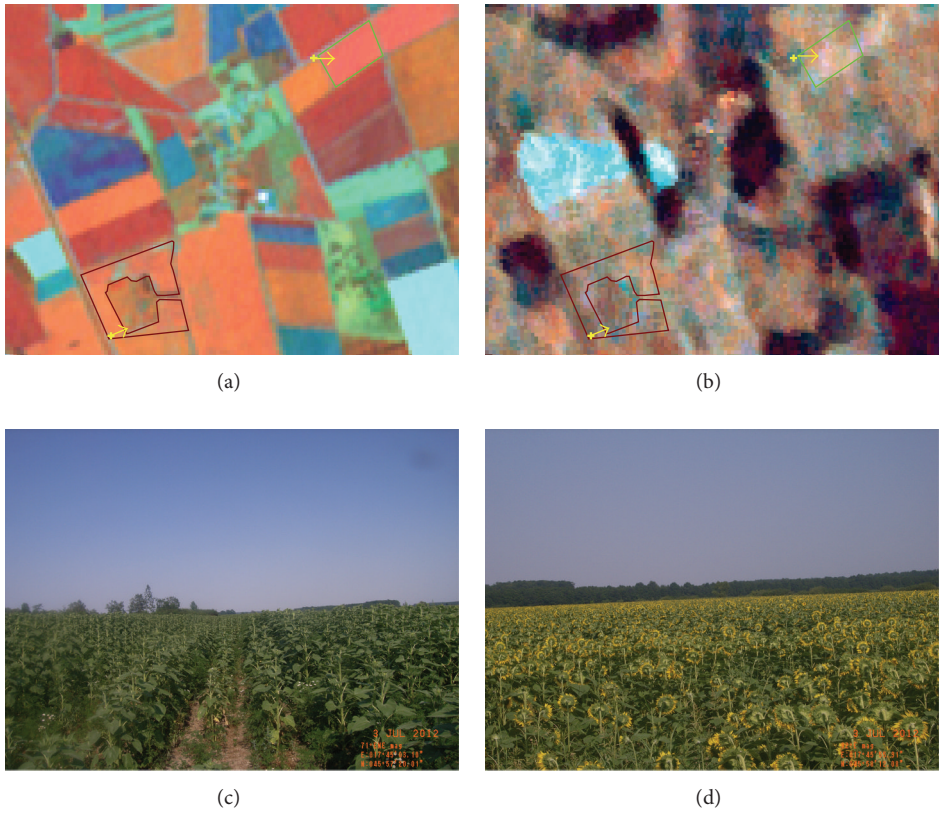

(a) (b) (c) (d)

Figure 6: Weed-infected (brown polygon) and control (green polygon) sunflower fields on IRS-P6 LISS (30/06/2012, R: NIR, G: SWIR, B: red) (a) and RADARSAT2 (17/06/2012, R: YAM_{odd}, G: SE, B: l2) satellite image composites (b) and photos taken on ground survey (3-4/7/2012) (c, d): weed-infected sunflower (c), control sunflower (d). Direction of the photos taken is shown by arrows.

B: l1) and photos taken on the spot (06–08/08/2012) as well (Figure 7).

State of maize is obvious on the photos taken on the spot. WCR damaged maize parcel with its stems leaned to each other randomly shows a rather disordered scenery. Contrarily, all the stems on maize parcel damaged by storm leaned according to wind direction, whilst control maize parcel looks well structured.

Difference between the three parcels can be detected on optical satellite composites acquired on 29/07/2012 and 19/08/2012, particularly in case of parcels damaged by storm. Difference between the 3 parcels is similarly apparent on the radar composite 26/07/2012, while no significant distinction appears any more on the radar composite 19/08/20.

2.4. Methodology Applied. Steps of preprocessing of optical satellite images are as follows:

(i) import,

(ii) geometric correction,

(iii) radiometric correction (ToA reflectance calculation),

(iv) generation of spectral indices (NDVI, NSI),

(v) intercalibration of spectral indices.

The spectral indices applied for our study were calculated from ToA reflectance instead of using surface reflectance; consequently these indices are not comparable between different years.

Reference fields' spectral index features Normalized Difference Vegetation Index (NDVI) and normalized special index (NSI) derived from optical images (SPOT4/5, Landsat TM7, IRS-P6/R2 LISS III, IRS-P6 AWiFS) are calculated from radiometric calibrated ToA reflectance values.

Definition of these indices is shown by

$$\begin{aligned} \mathrm{NDVI} &= 100 * \frac{\mathrm{NIR} - \mathrm{RED}}{\mathrm{NIR} + \mathrm{RED}}, \\ \mathrm{NSI} &= 100 * \frac{\mathrm{SWIR} - \mathrm{NIR}}{\mathrm{NIR} - \mathrm{RED}}, \end{aligned} \tag{1}$$

where NIR is the ToA reflectance in near infrared band, RED is the ToA reflectance in red band, and SWIR is the ToA reflectance in short wave infrared band.

The vegetation index, NDVI, describes the state and growth of vegetation, while NSI, based on our survey, serves characterization of spectral changes occurring in damaged fields. The different types of satellite images were intercalibrated, illustrated by Figure 8.

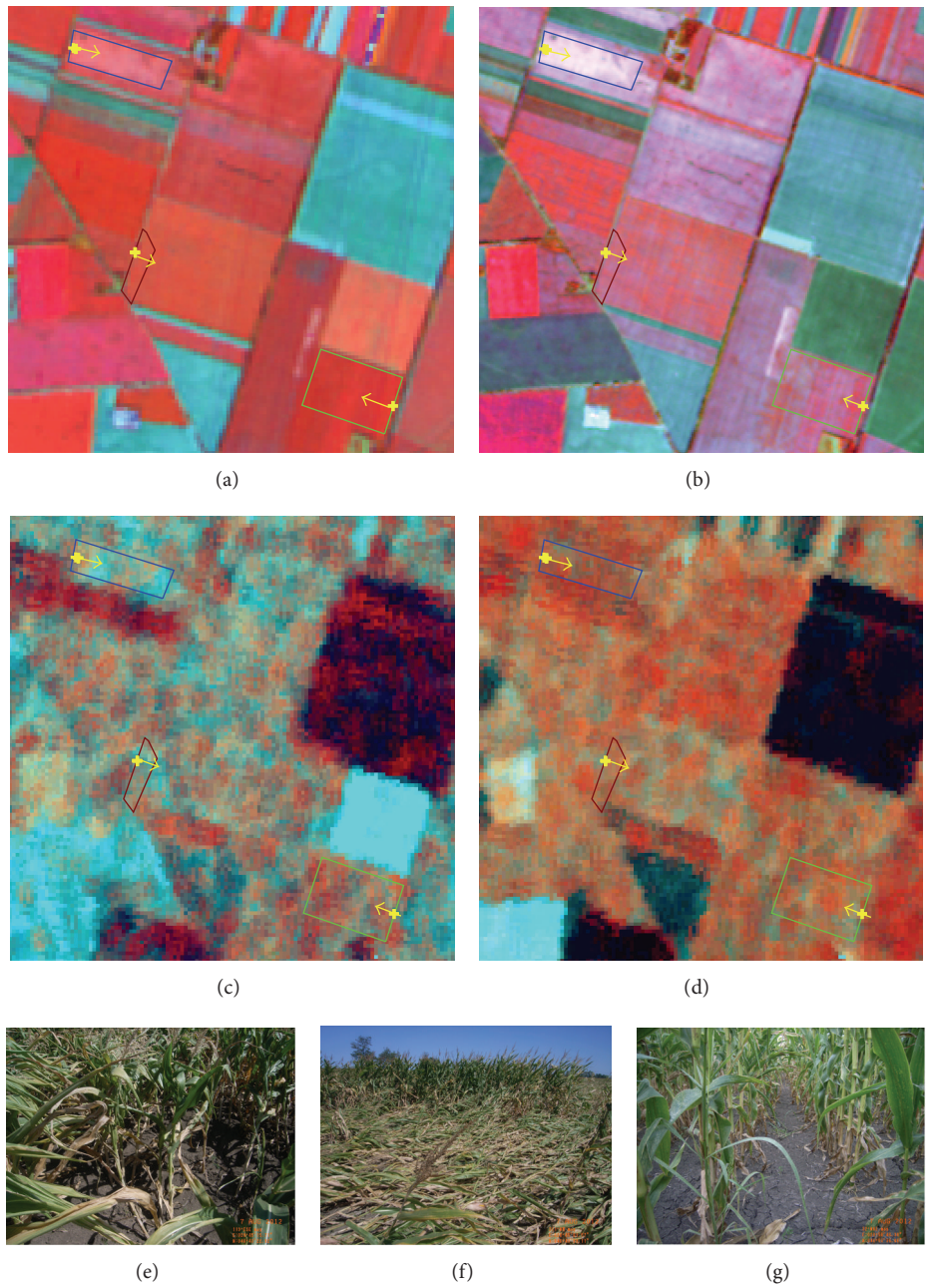

FIGURE 7: WCR-infected (brown polygon), storm (blue polygon) damaged, and control (green quadrangle) maize fields on SPOT4 (29/07/2012, R: NIR, G: SWIR, B: red) (a), SPOT5 (19/08/2012, R: NIR, G: SWIR, B: red) (b) optical and RADARSAT2 (26/07/2012, 19/08/2012, R: SE_p, G: SE_i, B: l1) (c, d) radar satellite image composites and photos taken on ground survey (6–8/08/2012) (e, f, g): WCR-infected (e), storm damaged (f), and control parcels (g). Direction of the photos taken is shown by arrows.

The well-known Landsat TM7 discontinuity (striping) errors were managed by intercalibrated spectral index derived from IRS P6/R2 AWiFS images having nearly similar acquisition date.

Preprocessing steps of RADARSAT2 data and radar features (assigned by light yellow) applied for our study are shown on Figure 9.

Calibrated backscattering coefficients (Sigma0) of standard quad-pol RADARSAT2 data were calculated by using NEST software. Polarimetric descriptors of these data were calculated by using Polsarpro software. Their definitions are described at [11]. Each of these types of software was developed by ESA. Two different types of decompositions (H/A/Alpha and Yamaguchi) and polarimetric features derived from those have been applied in our survey.

In our study the so called Shannon entropy based on H/A/Alpha decomposition of the coherency matrix [12] is one of the most important polarimetric descriptors. Natural

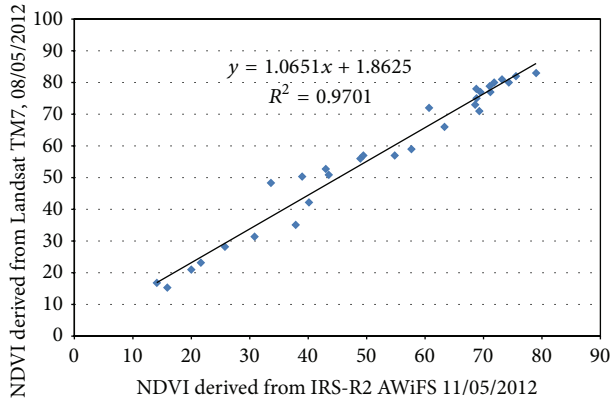

Figure 8: Intercalibration of NDVI values derived from IRS-R2 AWiFS and Landsat TM7.

Table 6: Characterisation of optical satellite images applied for Baranya site.

Acquisition date	Satellite	Spatial resolution (m)	Spectral resolution
01/05/2012	IRS-R2 LISS III	20	Green, red, NIR, SWIR
11/05/2012	IRS-R2 AWiFS	50	Green, red, NIR, SWIR
31/05/2012	Landsat TM7	30	Blue, green, red, NIR, SWIR1, SWIR2
16/06/2012	Landsat TM7	30	Blue, green, red, NIR, SWIR1, SWIR2
30/06/2012	IRS-P6 LISS III	20	Green, red, NIR, SWIR
02/07/2012	Landsat TM7	30	Blue, green, red, NIR, SWIR1, SWIR2
03/07/2012	IRS-R2 AWiFS	50	Green, red, NIR, SWIR
11/07/2012	Landsat TM7	30	Blue, green, red, NIR, SWIR1, SWIR2
28/07/2012	SPOT4	20	Green, red, NIR, SWIR
03/08/2012	Landsat TM7	30	Blue, green, red, NIR, SWIR1, SWIR2
05/08/2012	IRS-R2 LISS III	20	Green, red, NIR, SWIR
19/08/2012	Landsat TM7	30	Blue, green, red, NIR, SWIR1, SWIR2
20/08/2012	SPOT5	10	Green, red, NIR, SWIR
28/08/2012	Landsat TM7	30	Blue, green, red, NIR, SWIR1, SWIR2
10/09/2012	IRS-P6 LISS III	20	Green, red, NIR, SWIR

or agricultural damage often causes physical and visible disorders within the parcels. They can be characterized as follows: the polarization status of the transmitted and received pulses is known. The degree of polarization is influenced by the target. The so-called Shannon entropy (SE) can describe the ratio of "polarization scattering" above. Shannon entropy [13, 14] consists of two components:

$$\mathrm{SE} = \mathrm{SE}_i + \mathrm{SE}_p, \tag{2}$$

where SE is intrinsic degrees of coherence and SE_p is degrees of polarization.

Further important descriptors involved in our study are the components of Yamaguchi decomposition of the coherency matrix [15–17]. This type of decomposition technique can be applied for identification of scattering targets. It can account for the strength of different scattering mechanisms. Their components applied in this study are as follows: $\mathrm{YAM}_{\mathrm{odd}}$ for single scattering, $\mathrm{YAM}_{\mathrm{dbl}}$ for double bounce scattering, and $\mathrm{YAM}_{\mathrm{vol}}$ for volume scattering.

Efficiency and accuracy of these features were evaluated by statistical comparative analysis of reference crop fields. Based on the damaged (weed-infected, drought, WCR, or storm) and the healthy reference fields we analyzed the separability (significance) of the polarimetric descriptors of radar images mentioned above. Polarimetric descriptors of the reference fields are supposed to show normal distribution, so we derived the significance, t value calculated by the Welch test [18], and ranked the descriptors according to that. The Welch test is applicable here. The null hypothesis is the averaged values characterizing that damaged and control areas are equal.

Figure 10 shows the methodology applied. It is important to note that time series of radar and optical data have an equally significant role in identification of damage. Polarimetric descriptors derived from radar data contain a wide range of information. However they require adequate interpretation for each case. Therefore, we have to identify the crop type by the time series of optical satellite data. Interpretation of radar data should be implemented only for the mask generated based on the selected crop types. After

Table 7: Characterisation of radar satellite images applied for Baranya site.

Acquisition date	Satellite	Spatial resolution (m)	Polarisation	Wavelength (cm)	Incidence angle (°)	Beam	Pass
17/06/2012	RADARSAT2	20	Quad-pol	5.6	41.0–42.4	SQ22	Ascending
11/07/2012	RADARSAT2	20	Quad-pol	5.6	41.0–42.4	SQ22	Ascending
04/08/2012	RADARSAT2	20	Quad-pol	5.6	41.0–42.4	SQ22	Ascending
28/08/2012	RADARSAT2	20	Quad-pol	5.6	41.0–42.4	SQ22	Ascending

Table 8: Characterisation of optical satellite images applied for Békés site.

Acquisition date	Satellite	Spatial resolution (m)	Spectral resolution
03/07/2012	IRS-P6 LISS III	20	Green, red, NIR, SWIR
13/07/2012	Landsat TM7	30	Blue, green, red, NIR, SWIR1, SWIR2
29/07/2012	SPOT4	20	Green, red, NIR, SWIR
29/07/2012	Landsat TM7	30	Blue, green, red, NIR, SWIR1, SWIR2
08/08/2012	IRS-P6 LISS III	20	Green, red, NIR, SWIR
14/08/2012	Landsat TM7	30	Blue, green, red, NIR, SWIR1, SWIR2
19/08/2012	SPOT5	10	Green, red, NIR, SWIR

that, only one question has to be answered: whether the plant given is damaged or not.

3. Results and Discussion

3.1. Drought in Sunflower Fields, Csongrád Site. Figure 11 shows temporal progress of sunflower's average crop development curve derived from time series of optical satellite data, referred to as control parcels and parcels hit by drought. Horizontal lines stand for indicating standard deviation referring to each of the acquisition dates. The most significant difference takes place in the first decade of July. Difference decreases gradually by the first decade of August and then disappears. Therefore, it can be established that from the beginning of August, healthy and arid sunflower parcels are no longer separable by optical satellite images.

The temporal behaviour of NSI values (Figure 12) is reverse of NDVI.

Figure 13 shows the temporal development of sigma0 values of different polarization bands. In all bands the sigma0 values are lower in case of hit by drought. The higher difference between control and hit by drought areas is at the beginning of July in all bands particularly in HV one.

Figure 14 represents the separation of ellipses featured by control and hit-drought areas in two-dimensional space of sigma0 bands. We can see well the distinguishing is highest at the beginning of July like in Figure 11. The ellipses of controls are significantly upper-right at all dates. We can see similar distinguishing in H-Alpha space (Figure 15).

Figure 16 shows the result of separability analysis of polarimetric descriptors derived from RADARASAT2 satellite images acquired at different dates regarding reference sunflower parcels hit by drought and control ones. The one acquired on 8/7/2012 proved to be the most efficient in distinction. Although in case of each of the four acquisitions there exist such polarimetric descriptors which can distinguish these two states significantly.

It can be seen as well that not the same polarimetric descriptors show the highest efficiency at the dates given. Table 13 shows the ranking of polarimetric descriptors based on efficiency of separability or level of significance. It can be established that during the period of June to August components of Yamaguchi decomposition (mainly YAM_{vol} and YAM_{odd}) have notable role in distinguishing between sunflower parcels hit by drought and the control ones.

It is worth mentioning that component of "vol" is the one showing the most significant deviation (P value < 0.001) between July 8 and August 1, while the "odd" one has that in mid-June and end of August. It means that distinguishing these two states is dominated by volumetric scattering during the middle of the growing season (July-August), while single scattering has more important role at the beginning and end of the growing season (mid-June and August).

By evaluating both the optical and radar satellite time series data it can be established that the first decade of July is the most suitable date for distinguishing the sunflower parcels hit by drought from the control ones. According to Figure 17 those pixels of sunflower were identified as hit by drought, whose NDVI was less than 52 and l3 was less than 0.035.

The drought map was derived from Landsat TM7 (4/7/2012), from RADARSAT2 (8/7/2012) and from using both of them (Figure 18). The accuracy of these maps validated by reference data was almost the same (Figure 19).

3.2. Weed Infection in Sunflower Fields, Baranya Site. Figure 20 shows temporal progress of sunflower's average NDVI curve derived from time series of optical satellite data, referred to as the control (weed-free) parcels and parcels infected by weed. Horizontal lines indicate standard deviation referred to as each of the acquisition dates. In July deviation decreases appreciable while in August it starts to increase again. The largest deviation takes place in 2nd half

Table 9: Characterisation of radar satellite images applied for Békés site.

Acquisition date	Satellite	Spatial resolution (m)	Polarisation	Wavelength (cm)	Incidence angle (°)	Beam	Pass
26/07/2012	RADARSAT2	20	quad-pol	5.6	35.4–37.0	SQ16	Descending
19/08/2012	RADARSAT2	20	quad-pol	5.6	35.4–37.0	SQ16	Descending

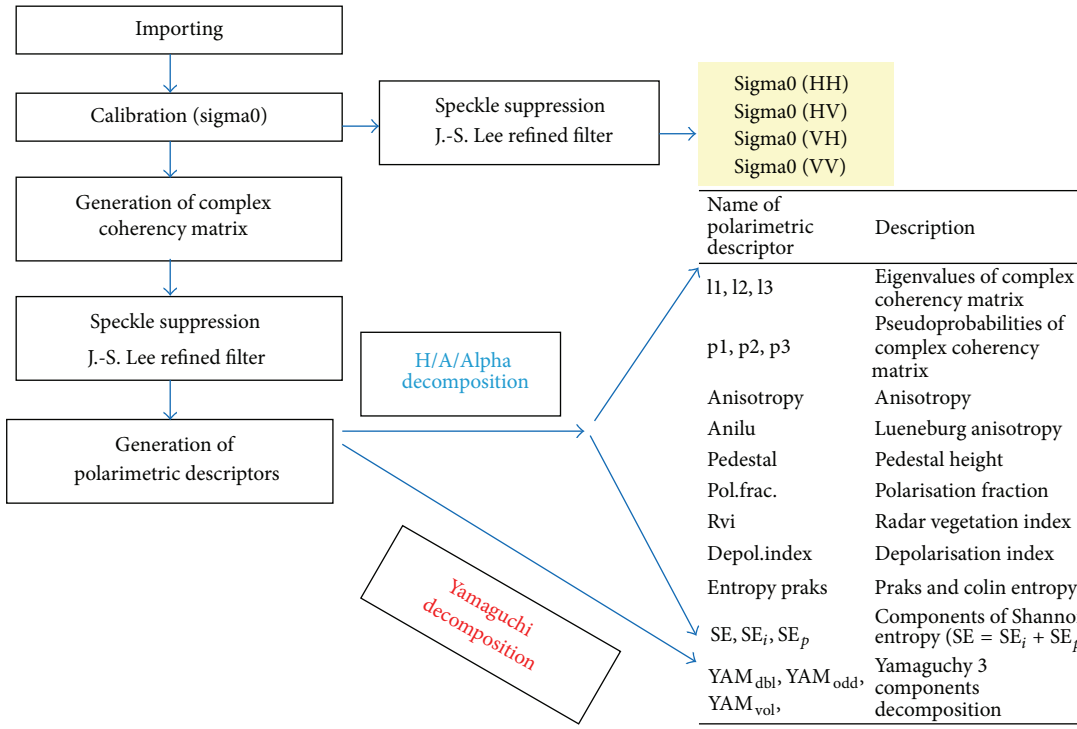

Figure 9: Preprocessing of RADARSAT2 satellite data and radar features applied for our study.

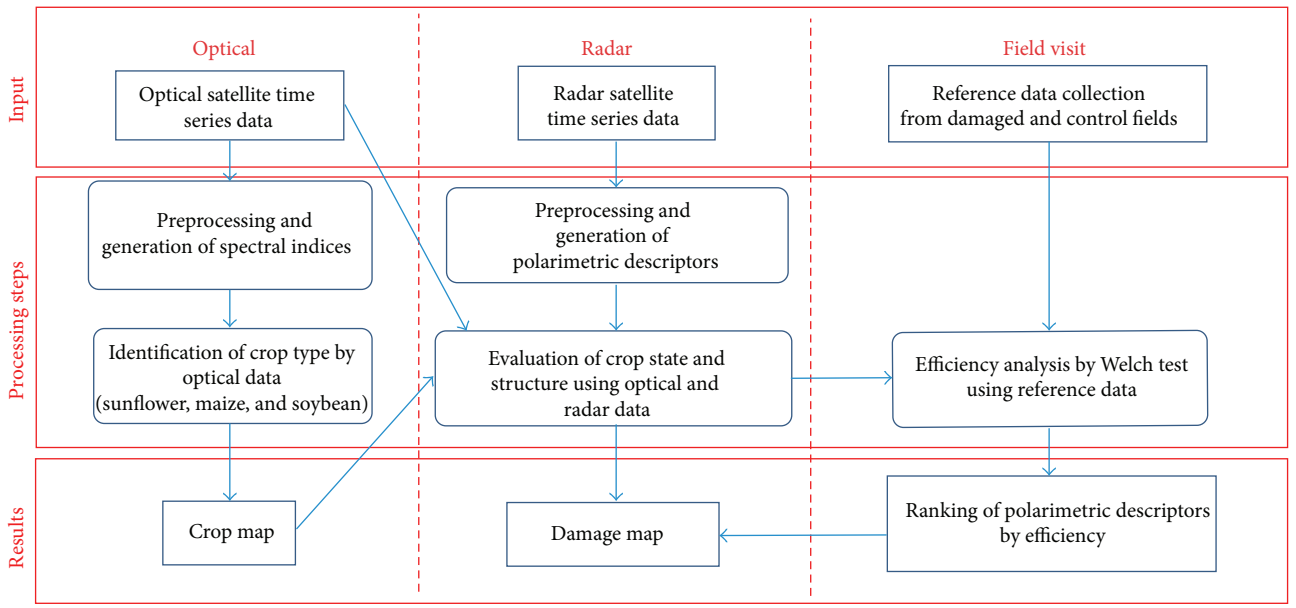

Figure 10: Sketch of methodology applied.

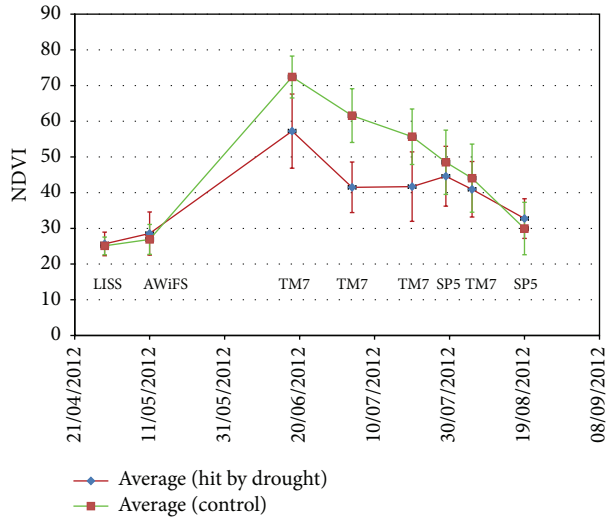

Figure 11: Average crop development curve based on NDVI values derived from time series of optical satellite data for sunflower hit by drought and control fields, Csongrád site. Vertical lines represent single standard deviation.

Table 10: Characterization of reference sunflower fields, Csongrád site.

Time period	Control		Hit by drought		Total	
	#field	Area (ha)	#field	Area (ha)	#field	Area (ha)
14-15/6/2012	5	79			5	79
3–5/7/2012	34	103	8	31.4	42	134
26/9/2012	5	11.8			5	12
Total	**44**	**194**	**8**	**31**	**52**	**225**

Table 11: Characterization of reference sunflower fields, Baranya site.

Time period	Weed-free		Weed-infected		Total	
	#field	Area (ha)	#field	Area (ha)	#field	Area (ha)
17/6/2012	2	18			2	18
3–7/7/2012	17	204	10	80	27	284
24–26/9/2012	11	67	13	51	24	118
Total	**30**	**289**	**23**	**131**	**53**	**420**

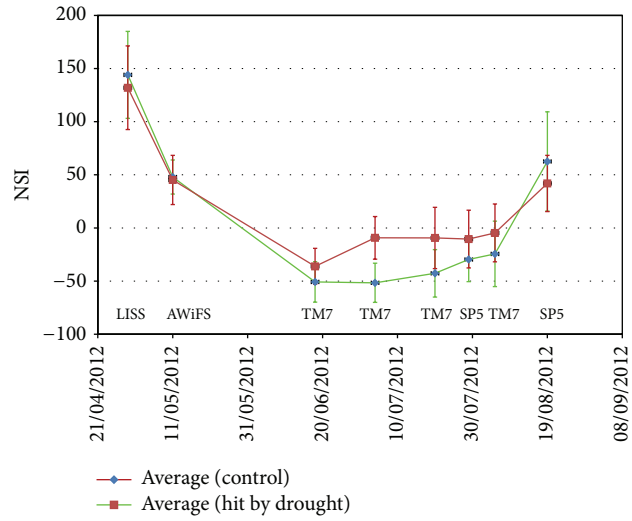

Figure 12: Average crop development curve based on NSI values derived from time series of optical satellite data for sunflower hit by drought and control fields, Csongrád site. Vertical lines represent single standard deviation.

of August. Therefore, it can be established that optical images acquired during that period are the most suitable for sorting out infected sunflower parcels from the control ones.

From Figures 20 and 21 we can see the NSI values have reverse behaviour as NDVI similar to the case above. The difference between weed-infected and weed-free areas is highest at end of August.

Figure 22 shows the temporal variation of sigma0 in different polarization cases weed-infected and weed-free areas. The graphs are similar in all polarization bands. The backscattered intensity of weed-infected and weed-free areas is changing at beginning of August. The weed-free is higher earlier and the weed-infected increased later. The highest difference between weed-free and weed-infected areas is at mid-June in particularly co-pol. bands. The trend of Shannon entropy (SE) is very similar (Figure 23).

The separability is well seen in the two-dimensional space of sigma0 co-pol. bands and H-Alpha bands too (Figures 24 and 25).

We have very interesting results from analysis above. We can find the weed-infected sunflower areas at mid-June by radar features. While we can distinguish the weed-infected areas by optical images only two months later, at the end of August.

Figure 26 represents the result of separability analysis of polarimetric descriptors derived from multitemporal radar

Table 12: Characterization of reference maize fields, Békés site.

Time period	Control		WCR damaged		Storm damaged		Total	
	#field	Area (ha)	#field	Area (ha)	#field	Area (ha)	#field	Area (ha)
6–8/8/2012	35	370	14	96	11	146	60	612
Total	**35**	**370**	**14**	**96**	**11**	**146**	**60**	**612**

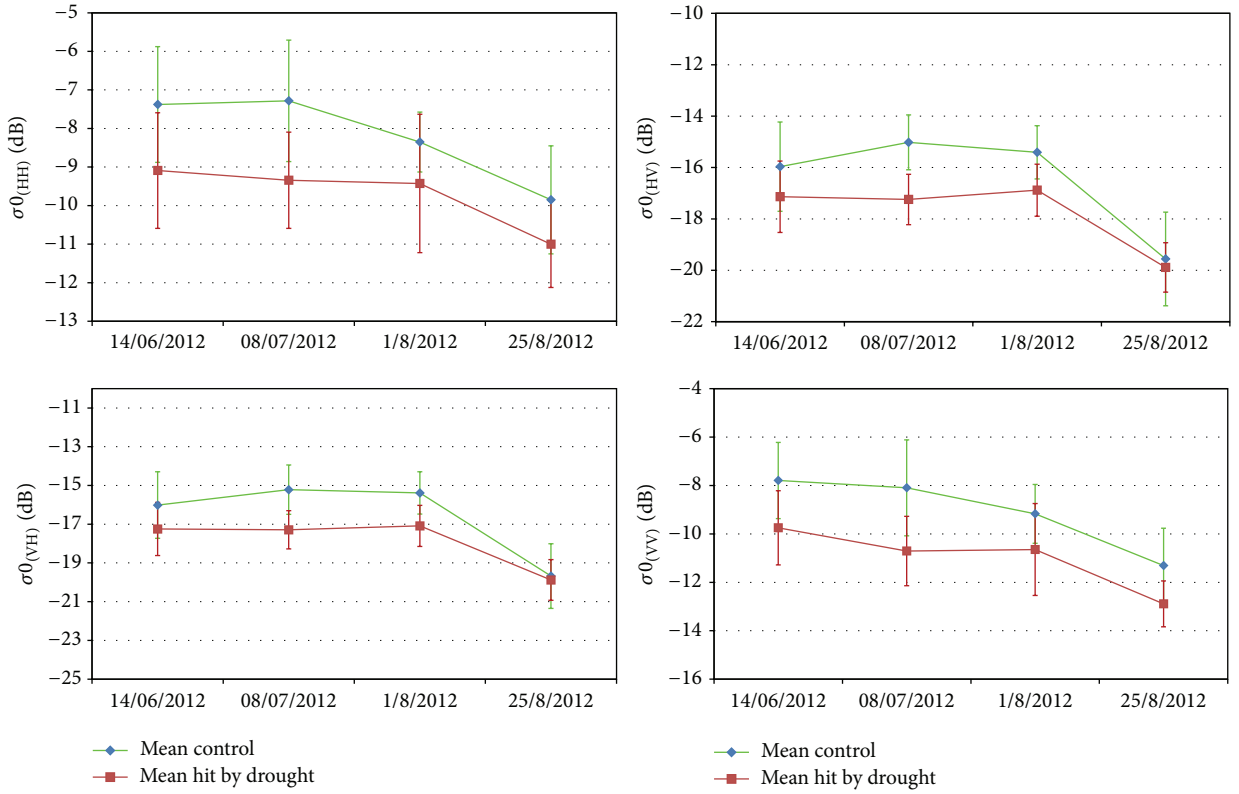

Figure 13: The temporal behavior of sigma0 bands of backscattered beam from sunflower (control and hit by drought area).

satellite data referred to as weed-free and weed-infected sunflower parcels. According to the graph, it is evidence that radar data acquired on 17/6/2012 is the most efficient in discrimination, while these two different statuses cannot be distinguished by analyzing radar data with other dates of acquisition about the area.

Hierarchy of polarimetric descriptors by their discrimination efficiency and level of significance is represented by Table 14. It is shown that components of Shannon entropy (SE, SE_i) ($P < 0.001$), odd and vol components of Yamaguchi decomposition ($0.001 < P < 0.01$), and eigenvalues of coherence matrix, l2 in particular (on level $P < 0.001$), have significant role in discrimination of the two distinct statuses for mid-June. However we could not find such polarimetric descriptors applicable in order to distinguish parcels of these two statuses in mid-July and late August. In case of radar satellite scene acquired in early August anisotropy and p2 descriptors ($0.01 < P < 0.05$) seemed to be significant in discrimination.

Based on evaluation of time series of both optical and radar satellite images it is evidence that weed infection in sunflower can be detected most efficiently by synergistic evaluation of optical data acquired in middle of August and radar data acquired in mid-June. According to Figure 27 sunflower parcels having value of NDVI > 35 in middle of August and Shannon entropy < −1 in mid-June are expected to be infected.

We made weed maps in many different ways shown in Table 15. The overall accuracy of these maps is shown in the last column of Table 15. Figure 28 shows the map detailed in bold row of Table 15, and the accuracy of the map is almost 90%.

The accuracy of the processes was validated with reference data collection by field visit. The overall accuracy (%) and the Kappa value (%) [19] of different weed-infection maps are shown by Figure 29.

The accuracy of identification of weed-infected and weed-free areas was studied by averages of Hellden and Short measures [20], Figure 30.

3.3. WCR and Storm Damage in Maize Fields, Békés Site. The average temporal change of NDVI time series of healthy

Table 13: Ranking of polarimetric descriptors based on significance (t) calculated by Welch test, referred to as sunflower hit by drought and control fields, Csongrád site.

Sign. (t) and P value	Date of polarimetric descriptors			
	14/06/2012	08/07/2012	01/08/2012	25/08/2012
>3.8 <0.001	—	l3, l1, YAM_{vol}, SE, l2, SE_i	YAM_{vol}	YAM_{odd}, l1
2.9–3.8 0.001–0.01	—	YAM_{odd}	l2, l3	—
2.1–2.9 0.01–0.05	YAM_{odd}, l1, SE_i ped, p3, rvi, polfrac, SE, SE_p, p1, l2, anilu	—	SE	SE, p1 anilu, SE_p

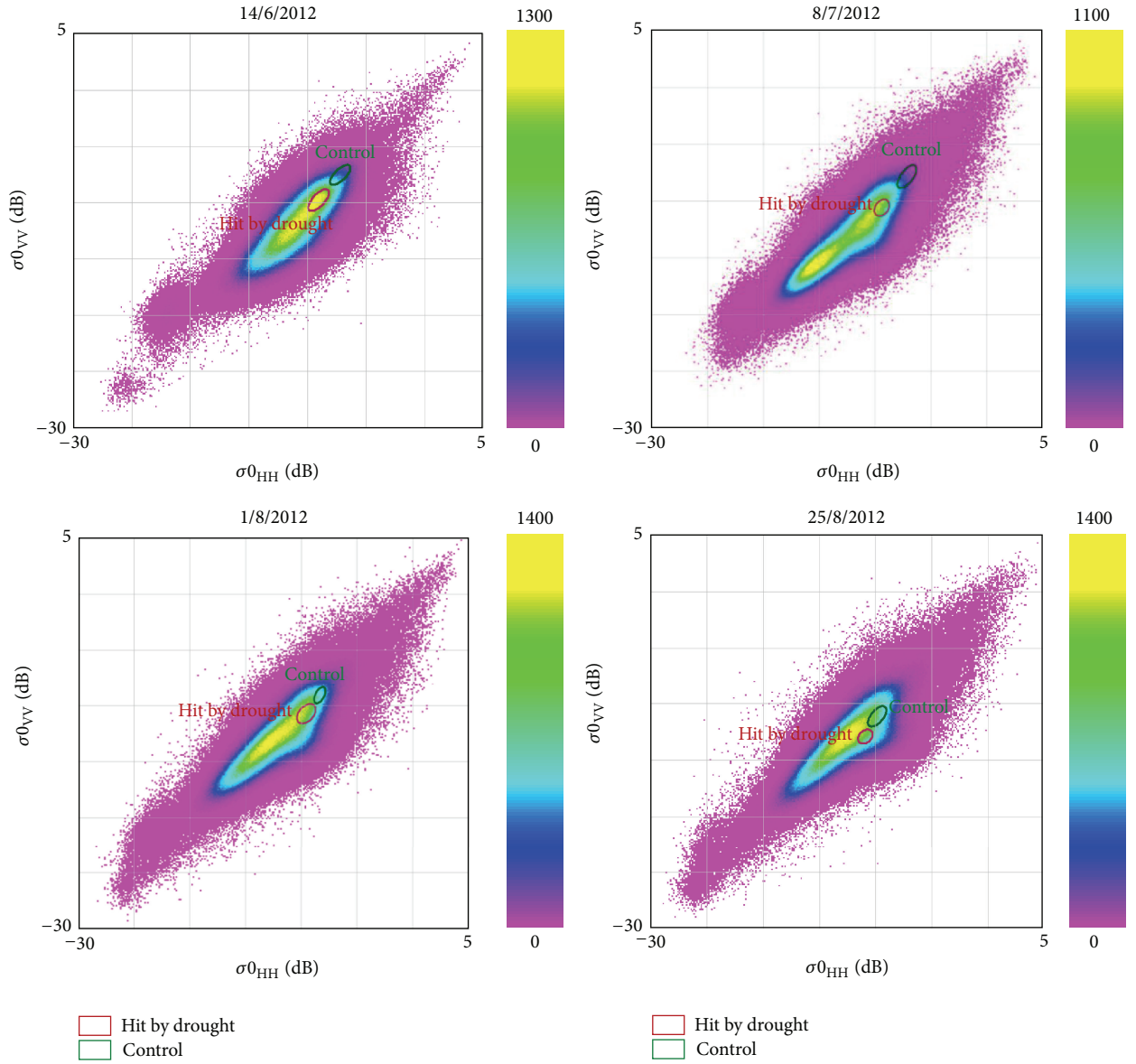

Figure 14: Separability of hit-drought and control areas in two-dimensional space of sigma0 co-pol. bands at different dates.

reference maize parcels to the ones damaged by Western Corn Rootworm and the storm which occurred on July 7 can be seen in Figure 31. Vertical lines represent standard deviation relevant to definite data. Figure 31 shows that no remarkable deviation among the three diverse states can be detected. Deviation from the control parcels increases gradually during the period between July 10 and mid-August, particularly after the storm occurred. Therefore, maize parcels damaged by storm and Western Corn Rootworm can be separated from the control ones most efficiently by evaluation of optical

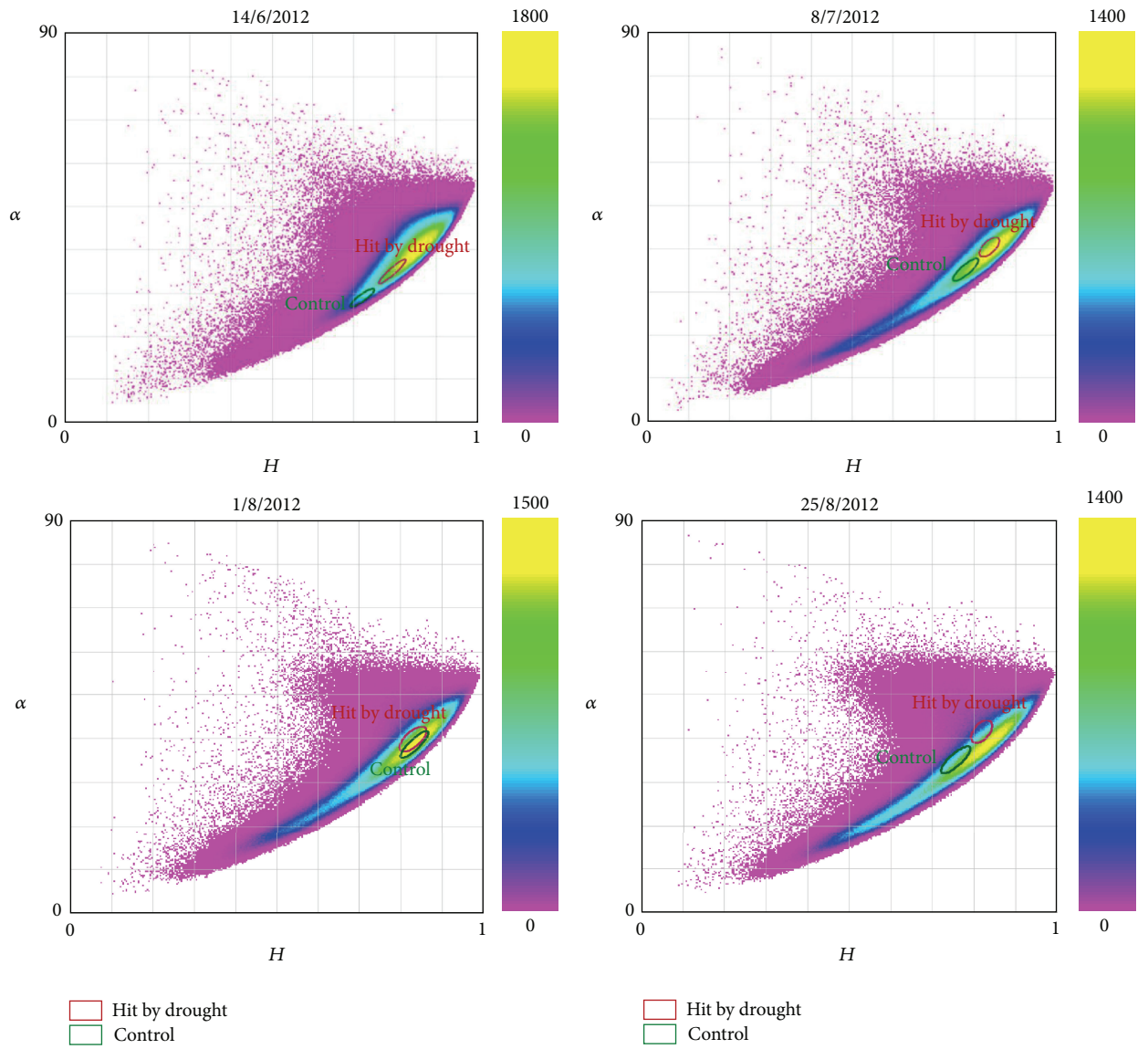

Figure 15: Separability of hit-drought and control areas in two-dimensional space of H-Alpha polarimetric descriptors at different dates.

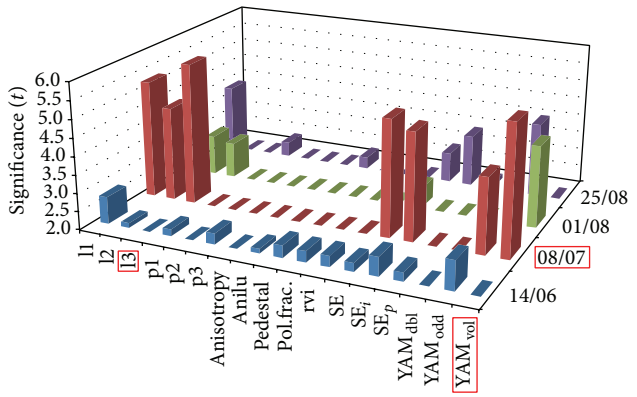

Figure 16: Result of separability analysis of sunflower hit by drought and control fields, Csongrád site.

Table 14: Ranking of polarimetric descriptors based on significance calculated by Welch test, weed-infected and weed-free sunflower fields, Baranya site.

Sign. and P value	Polarimetric descriptors			
	17/06/2012	11/07/2012	04/08/2012	28/08/2012
>3.8 <0.001	SE, l2 SE_i	—	—	—
2.9–3.8 0.001–0.01	YAM_{vol}, YAM_{odd} l3, l1	—	—	—
2.1–2.9 0.01–0.05	SE_p	—	Anisotropy, p2	—

satellite data acquired between the end of July and mid-August.

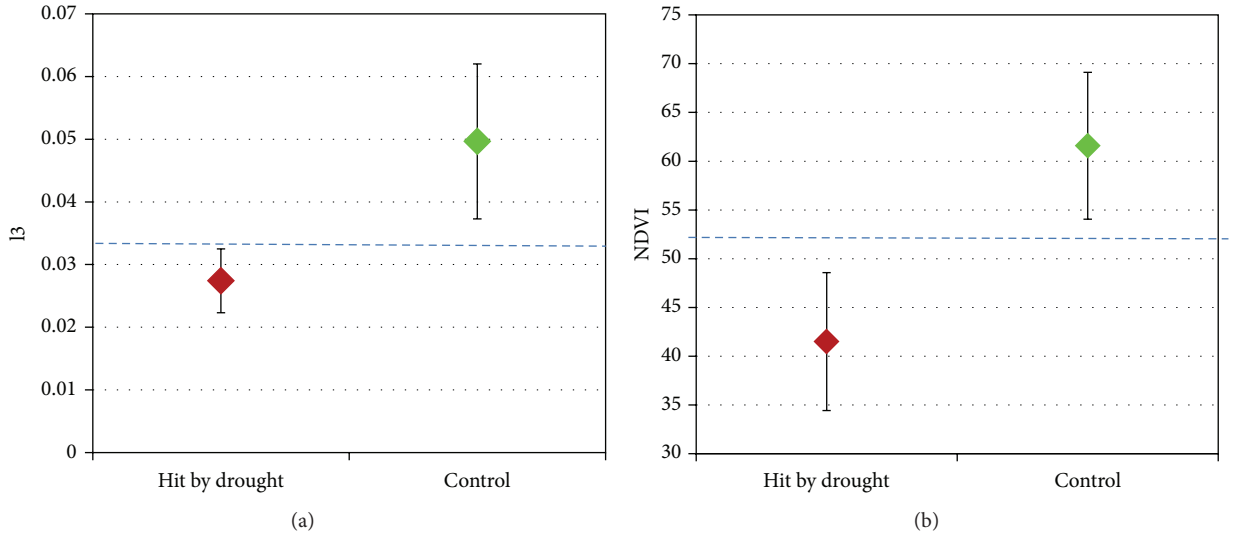

Figure 17: Average deviation of damaged (hit by drought) and healthy (control) reference parcels based on l3 derived from RADARSAT2 (08/07/2012), $P < 0.001$ (a). Average deviation of damaged (hit by drought) and healthy (control) reference sunflower fields based on NDVI derived from Landsat TM7 (04/07/2012), $P < 0.001$ (b). Vertical lines represent single standard deviation.

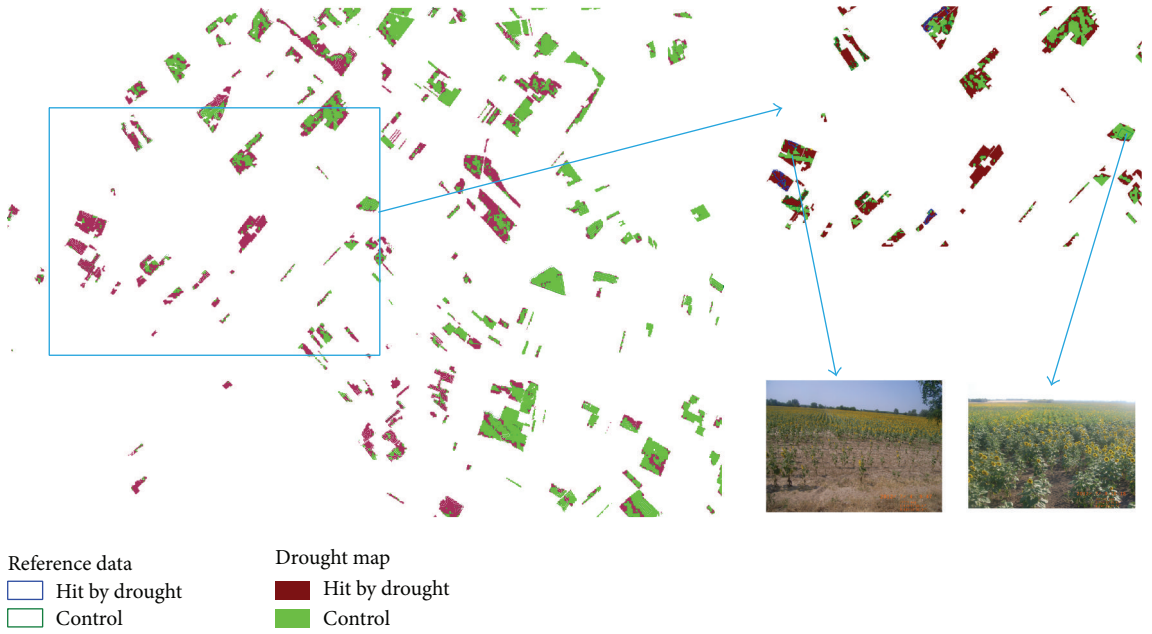

Figure 18: Drought map of sunflower parcels derived from integrated evaluation of Landsat TM7 (4/7/2012) and RADARSAT2 (8/7/2012) and the reference sunflower parcels.

Analogue can be observed in Figure 32 on which identification of the three different states can be followed by the help of NSI index derived from optical satellite data. Based on that the most efficient feature is the one derived from optical satellite image acquired in mid-August.

The mentioned three states of the maize parcels are represented in the two-dimensional space of co-pol bands of sigma0 (Figure 33).

Figure 34 represents result of separability analysis of polarimetric descriptors derived from multitemporal radar satellite data referred to as maize parcels damaged by larvae of Western Corn Rootworm. According to Figure 34, radar data acquired on July 26, 2012 is proved to be more efficient in discrimination to the one acquired on August 19, 2012. Table 16 shows ranking of polarimetric descriptors based on discriminating efficiency of level of significance. It reveals that odd component of Yamaguchi decomposition and p component of Shannon entropy (SE_p) have the most important role in it (on significance level $0.001 < P < 0.01$). Although, in case of mid-August radar data there are

Table 15: Characterization of weed maps derived from radar and optical satellite data for sunflower parcels.

Basis of weed map	Type	#dates	Last date	Conditions for identification of weed infection	Overall (%)
RS2, 17/6/2012	Radar	1	17/6/2012	SE < −1	61.1
SPOT4, 28/7/2012	Optical	1	28/7/2012	NDVI > 60	72.8
LISS, 5/8/2012	Optical	1	5/8/2012	NDVI > 50	78.4
SPOT5, 20/8/2012	Optical	1	20/8/2012	NDVI > 35	83.0
SPOT4, 28/7/2012 + LISS, 5/8/2012	Optical	2	5/8/2012	NDVI1 > 60 and NDVI2 > 50	78.8
RS2_17/6/2012 + RS2_11/7/2012	Radar	2	11/7/2012	SE1 < −1 and SE2 < −1	78.9
RS2_17/6/2012 + RS2_11/7/2012 + SPOT4, 28/7/2012 + LISS, 5/8/2012	**Radar + optical**	**2-2**	**5/8/2012**	**SE1 < −1 and SE2 < −1 and NDVI1 > 60 and NDVI2 > 50**	**89.7**
RS2_17/6/2012 + SPOT4_28/7/2012	Radar + optical	1-1	28/7/2012	SE < −1 and NDVI > 60	83.9
RS2_17/6/2012 + LISS_5/8/2012	Radar + optical	1-1	5/8/2012	SE < −1 and NDVI > 50	86.7
RS2_17/6/2012 + SPOT5_20/8/2012	*Radar + optical*	*1-1*	*20/8/2012*	*SE < −1 and NDVI > 35*	*91.3*

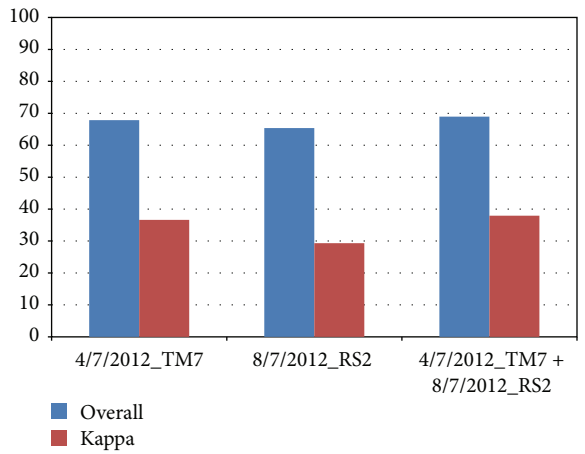

Figure 19: Result of accuracy assessment of sunflower's drought map.

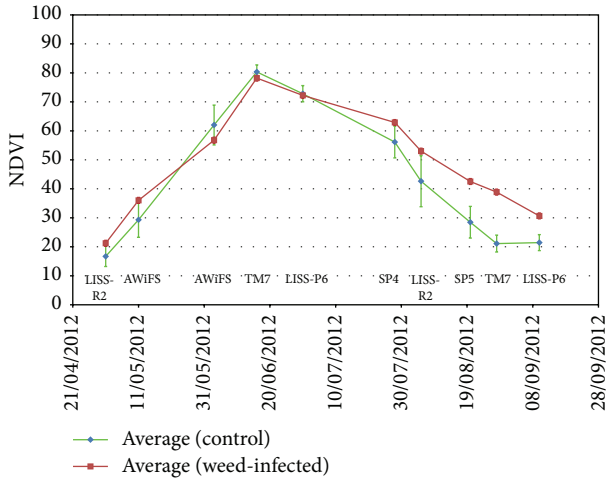

Figure 20: NDVI derived from optical satellite data for weed-infected and control sunflower fields, Baranya site. Vertical lines represent single standard deviation. LISS-R2: IRS-R2 LISS III, AWiFS: IRS-R2 AWiFS, TM7: Landsat TM7, LISS-P6: IRS-P6 LISS III, SP4: SPOT4, and SP5: SPOT5.

Table 16: Ranking of polarimetric descriptors based on significance calculated by Welch test, WCR damaged and control maize fields, Békés site.

Sign. and P value	Date of polarimetric descriptors	
	26/07/2012	19/08/2012
3–3.9 0.001–0.01	YAM_{odd}, SE_p	—
2.1–3 0.01–0.05	entropy praks, l1, depol.index, p1, SE_i pedestal, anilu, SE	YAM_{dbl}, pol.frac., rvi, p3

Table 17: Ranking of polarimetric descriptors based on significance calculated by Welch test, storm damaged and control maize fields, Békés site.

Sign. and P value	Date of polarimetric descriptors	
	26/07/2012	19/08/2012
>3.9 <0.001	l1, SE_i	—
2.8–3.9 0.001–0.01	YAM_{odd}, SE, l2, SE_p	YAM_{dbl}, l2, SE, SE_i
2.1–2.8 0.01–0.05	Entropy praks, depol.index, p1, anilu, pedestal, pol.frac., rvi, p3	l3, l1

such polarimetric descriptors (YAM_{dbl}, pol.frac., rvi, and p3), suitable to separate different states significantly. However, this application is confined to significance level $0.01 < P < 0.05$.

Figure 35 represents result of separability analysis of polarimetric descriptors derived from multitemporal radar satellite data referred to as maize parcels damaged by storm and control parcels. According to the figure, radar data acquired on July 26, 2012 is proved to be more efficient in discrimination compared to the one acquired on August 19, 2012. Table 17 shows ranking of polarimetric descriptors based on discriminating efficiency of level of significance. The table reveals that the first eigenvalue of coherence matrix (l1) and i component of Shannon entropy (SE_i) have the most

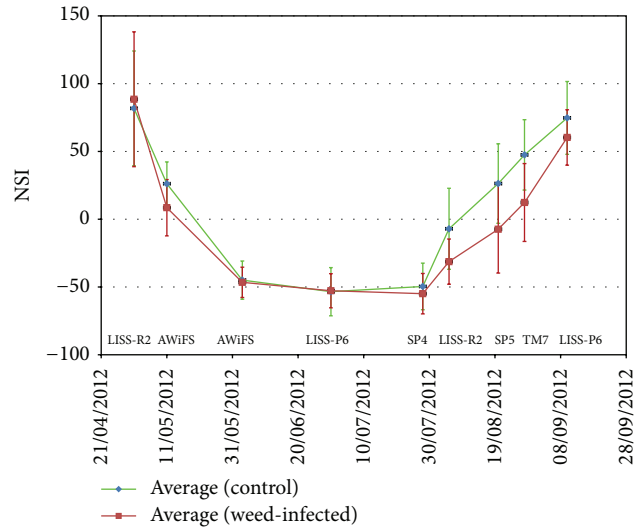

FIGURE 21: NSI derived from optical satellite data regarded to weed-infected and control sunflower fields, Baranya site. Vertical lines represent single standard deviation. LISS-R2: IRS-R2 LISS III, AWiFS: IRS-R2 AWiFS, TM7: Landsat TM7, LISS-P6: IRS-P6 LISS III, SP4: SPOT4, and SP5: SPOT5.

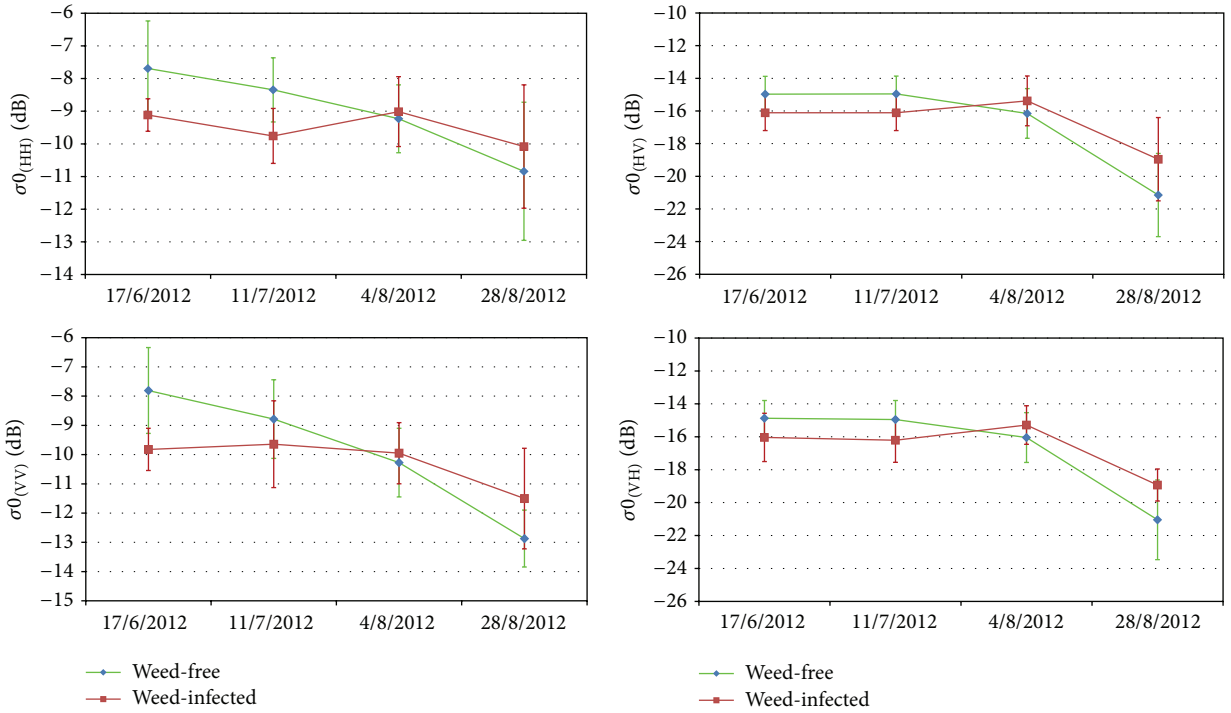

FIGURE 22: Temporal development of sigma0 values in different polarization bands, Baranya site.

important role (on $P < 0.001$ significance level). Although in case of radar data acquired in mid-August there are such polarimetric descriptors (YAM_{dbl}, l2, SE, and SE_i), suitable to separate these two different states significantly; however their application is confined to significance level $0.001 < P < 0.01$.

Figure 36 represents result of separability analysis of polarimetric descriptors derived from multitemporal radar satellite data referred to as maize parcels damaged by storm parallel to those damaged by larvae of Western Corn Rootworm. According to the figure it is obvious that based on radar data acquired on July 26, 2012 these two different cases cannot be separated significantly. We were able to find a few polarimetric descriptors which were able to separate these cases from each other, although only restricted to significance level $0.01 < P < 0.005$. Table 18 shows ranking of polarimetric descriptors based on discriminating efficiency level of significance referred to as certain dates of acquisition. The table reveals that there exist such polarimeric descriptors

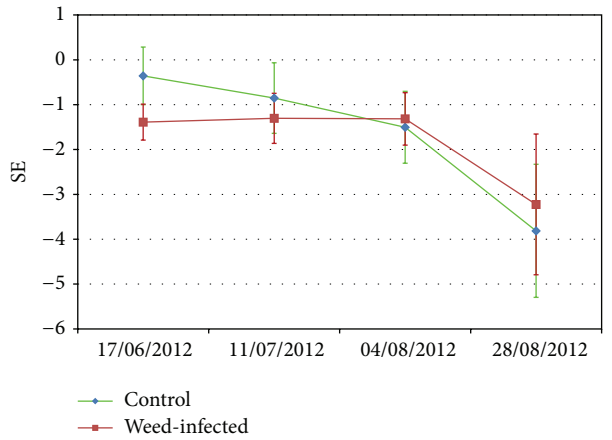

Figure 23: Temporal development of SE polarimetric descriptor, Baranya site.

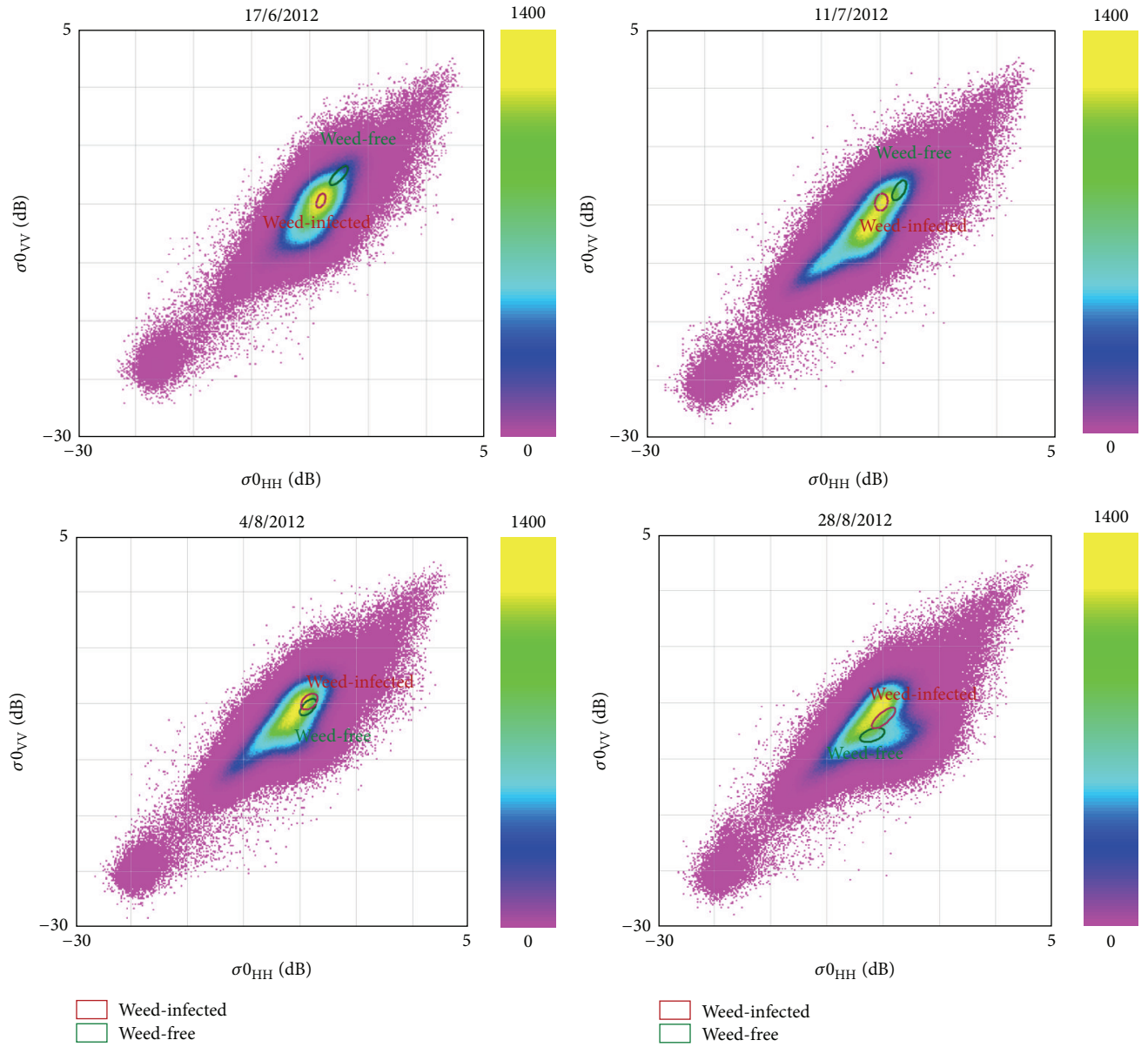

Figure 24: Separability of weed-infected and weed-free areas in two-dimensional space of sigma0 co-pol. bands at different dates, Baranya site.

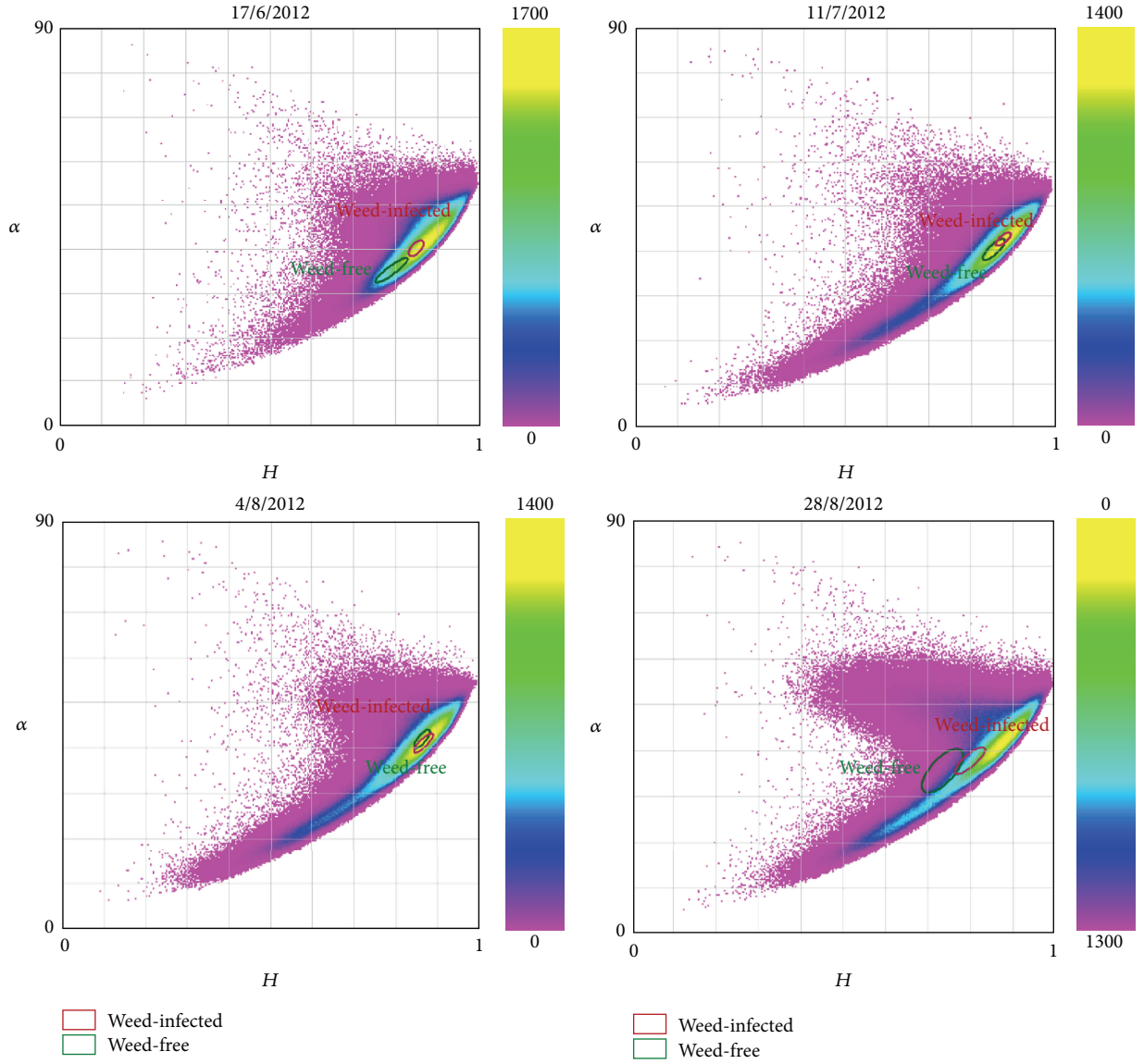

Figure 25: Separability of weed-infected and weed-free areas in two-dimensional space of H-Alpha polarimetric descriptors at different dates, Baranya site.

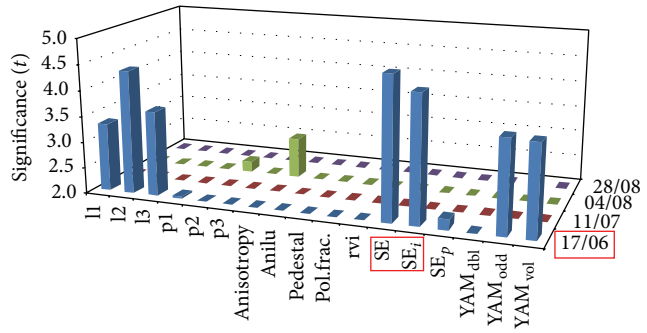

Figure 26: Result of separability analysis of discriminating weed-infected and weed-free sunflower fields, Baranya site.

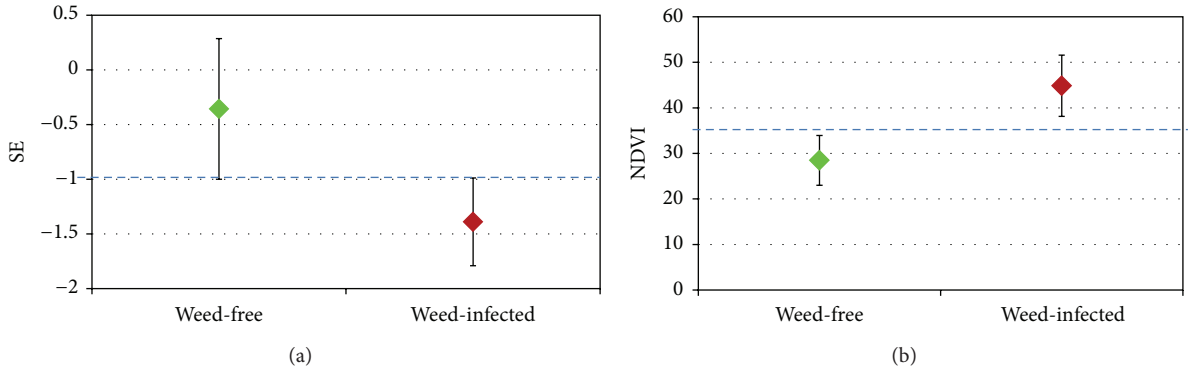

Figure 27: Average discrimination of weed-infected and weed-free reference sunflower fields based on SE derived from RADARSAT2 (17/06/2012), $P < 0.001$ (a). Average discrimination of weed-infected and weed-free reference sunflower fields based on NDVI derived from SPOT5 (20/08/2012), $P < 0.001$ (b). Vertical lines represent single standard deviation.

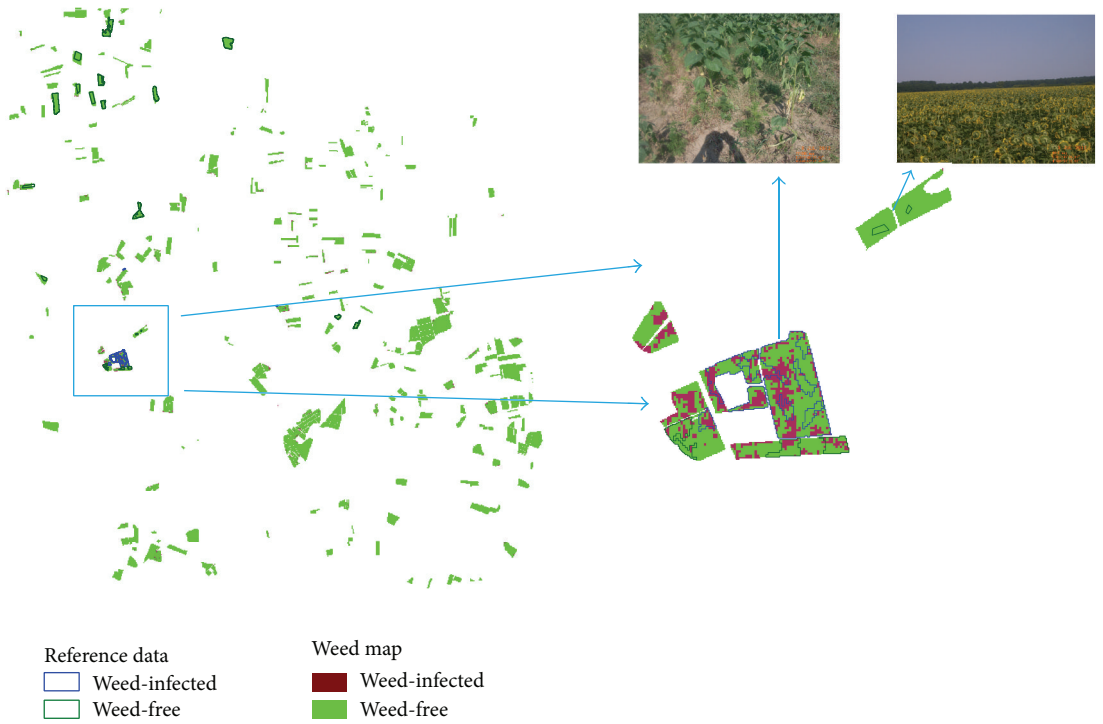

Figure 28: Weed infection map of sunflower parcels, created from optical and radar images.

(l3, l2, SE, and YAM_{vol}), eligible to separate significantly these two kinds of conditions, although these can be applicable only restricted to significance level $0.01 < P < 0.05$. However, in case of radar satellite data acquired during the last decade of July, none of the polarimetric descriptors were able to separate these cases at least by significance level $P = 0.05$.

Based on evaluation of time series of optical and radar satellite data alike, it can be established that identification of maize damaged by larvae of Western Corn Rootworm can be the most efficient by synergistic evaluation of those optical and radar satellite data acquired around the end of July. Taking Figures 37(a) and 38(a) into consideration those maize parcels are likely to be damaged where NDVI < 53 derived from IRS-P6 LISS III (08/08/2012) and $YAM_{odd} > -7.7$ derived from RADARSAT2 (26/07/2012). Similarly, maize parcels damaged by storm to healthy control parcels can be

Table 18: Ranking of polarimetric descriptors based on significance calculated by Welch test, WCR and storm damaged maize fields, Békés site.

Sign. and P value	Date of polarimetric descriptors	
	26/07/2012	19/08/2012
2.1–2.8 0.01–0.05	—	l3, l2, SE, YAM_{vol}

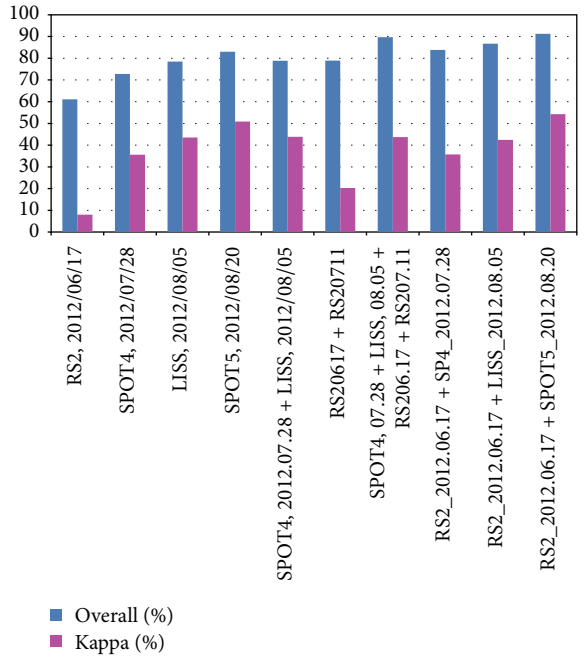

Figure 29: Result of general accuracy assessment of weed maps of sunflower parcels.

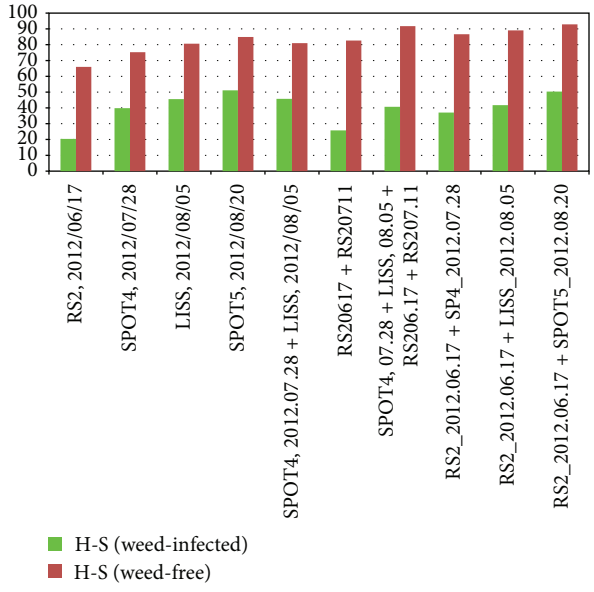

Figure 30: Result of accuracy assessment of the categories of weed maps indicated by average of measures defined by Hellden and Short.

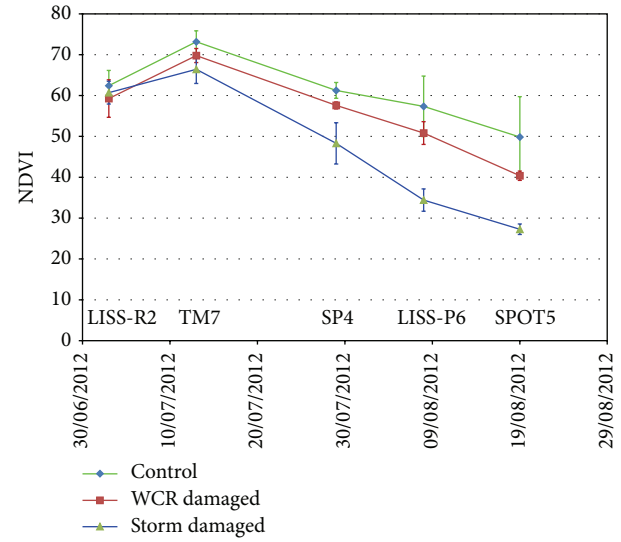

Figure 31: NDVI derived from optical satellite data for WCR and storm damaged and control maize fields, Békés site. Vertical lines represent single standard deviation. LISS-R2: IRS-R2LISS III, TM7: Landsat TM7, LISS-P6: IRS-P6 LISS III, SP4: SPOT4, and SP5: SPOT5.

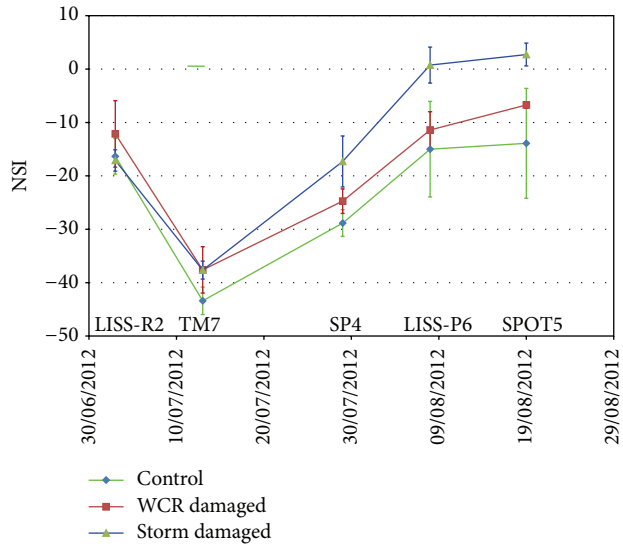

Figure 32: NSI derived from optical satellite data for WCR and storm damaged and control maize fields, Békés site. Vertical lines represent single standard deviation. LISS-R2: IRS-R2LISS III, TM7: Landsat TM7, LISS-P6: IRS-P6 LISS III, SP4: SPOT4, and SP5: SPOT5.

separated most efficiently based on synergistic evaluation of optical and radar satellite data acquired between the end of July and mid-August. Based on Figures 37(b) and 38(b) those maize parcels are the most likely to be damaged by storm where NSI < -3 derived from SPOT5 (19/08/2012) and l1 $>$ 0.24 derived from RADARSAT2 (26/07/2012).

Based on Figures 37(c) and 38(b) differently damaged corn fields can be separated by NSI index derived from SPOT5 (19/08/2012) and l3 value derived from RADARSAT2 (19/08/2012) data. In case NSI > -3 and l3 < 0.022, damage by storm is more likely, while in NSI < -3 or l3 > 0.022 maize field is damaged by Western Corn Rootworm otherwise.

The identification of damaged maize parcels was carried out by coevaluating the odd component of Yamaguchi decomposition derived from the RADARSAT2 (26/7/2012) and the NDVI calculated from the IRS-P6 LISS III (8/8/2012). The separation of the two damaged states was made by

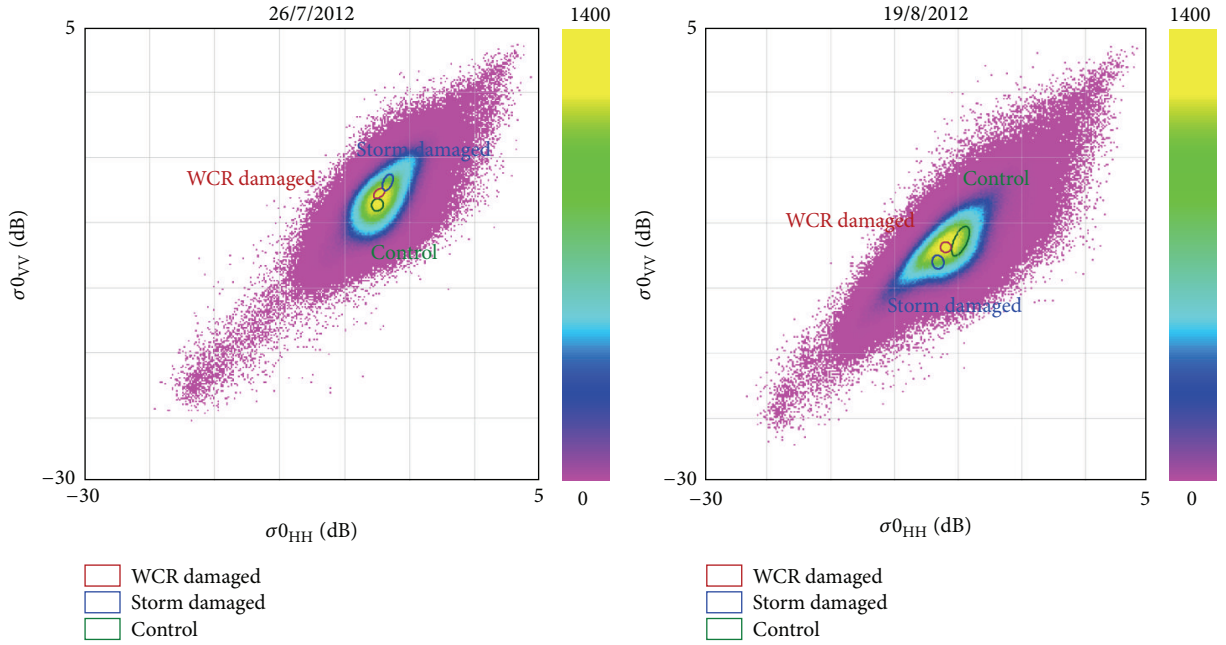

Figure 33: The ellipse positions of three states of the maize parcels in the co-pol. bands sigma0 space at different date.

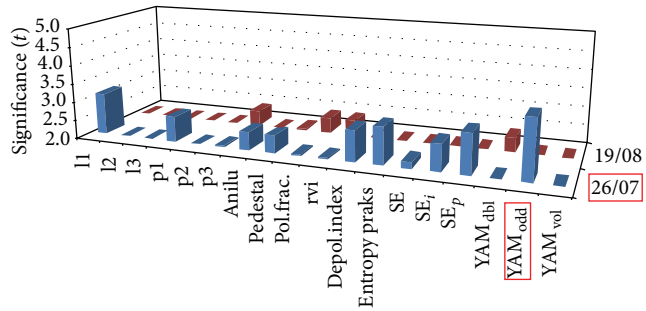

Figure 34: Result of separability analysis of WCR damaged and control fields, Békés site.

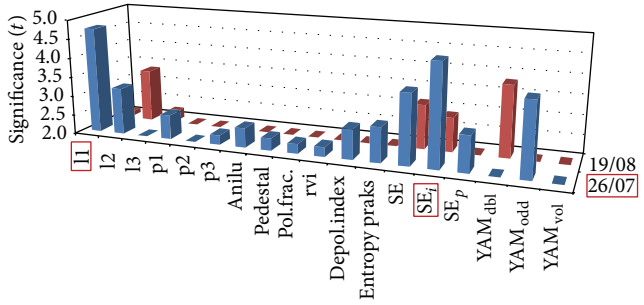

Figure 35: Result of separability analysis of discriminating storm damaged and control maize fields, Békés site.

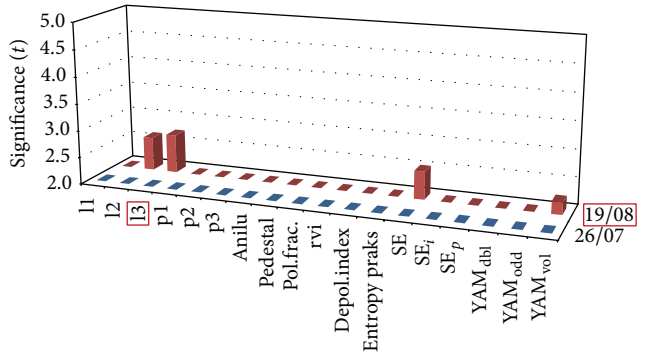

Figure 36: Result of separability analysis of storm and WCR damaged maize fields, Békés site.

the coevaluation of l3 derived from RADARSAT2 (19/8/2012) and NSI derived from SPOT5 (19/8/2012). The created damaged map is shown in Figure 39.

The damage map was compared to the reference data from field visit; we found the overall accuracy is about 75%.

4. Conclusions

In most cases, damage in croplands does not induce any notable spectral changes; therefore, they cannot be traceable

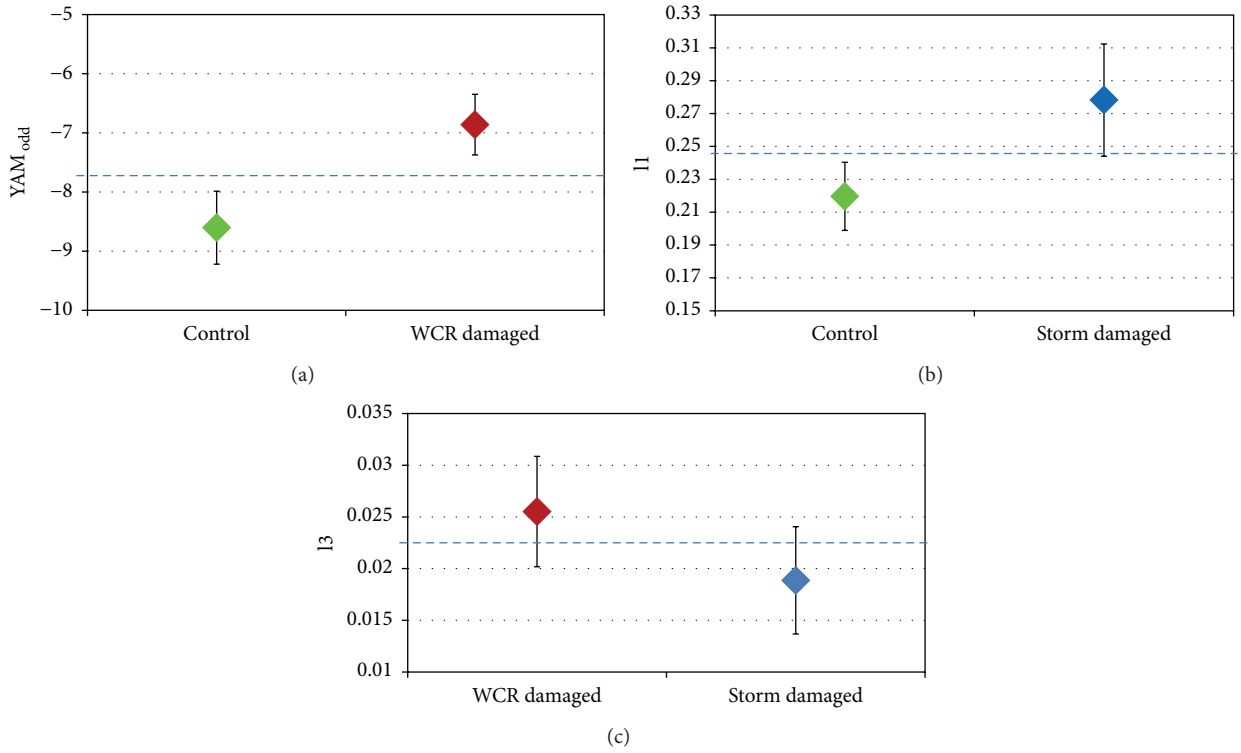

Figure 37: Average discrimination of WCR damaged and control reference maize fields based on YAM_{odd} derived from RADARSAT2 (26/07/2012), $P < 0.001$ (a). Average discrimination of storm damaged and control reference maize fields based on l1 derived from RADARSAT2 (26/07/2012), $P < 0.001$ (b). Average discrimination of WCR and storm damaged reference maize fields based on l3 derived from RADARSAT2 (19/08/2012), $0.01 < P < 0.05$ (c). Vertical lines represent single standard deviation.

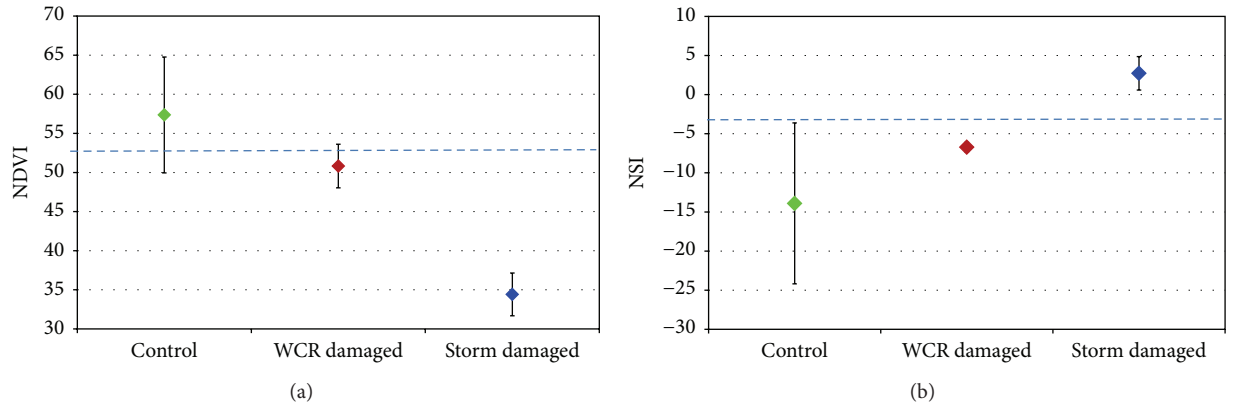

Figure 38: Average discrimination of WCR, storm damaged and control reference maize fields based on NDVI derived from IRS-P6 LISS III (08/08/2012), $P < 0.001$ (a). Average discrimination of WCR, storm damaged and control reference maize fields based on NSI derived from SPOT5 (19/08/2012), $P < 0.001$ (b). Vertical lines represent single standard deviation.

in optical range. However, polarimetric radar observation is applicable to identify changes in case they are accompanied by structural alterations. It is detectable that, in case of WCR and storm damage in corn, drought or weed infection in sunflower can be identified by polarimetric radar satellite images. We determined the most suitable polarimetric descriptors for characterising the abovementioned types of damage and their optimal time periods.

Synergistic application of radar and optical satellite data brings significant improvement in accuracy of identification of detecting damage accompanied by geometrical structure changes of vegetation. The most important output of our study is to emphasize the importance and to select those polarimetric descriptors which fit most of all the task given. For this express purpose a statistical method has already been developed. Importance of the method lies in the numbers of

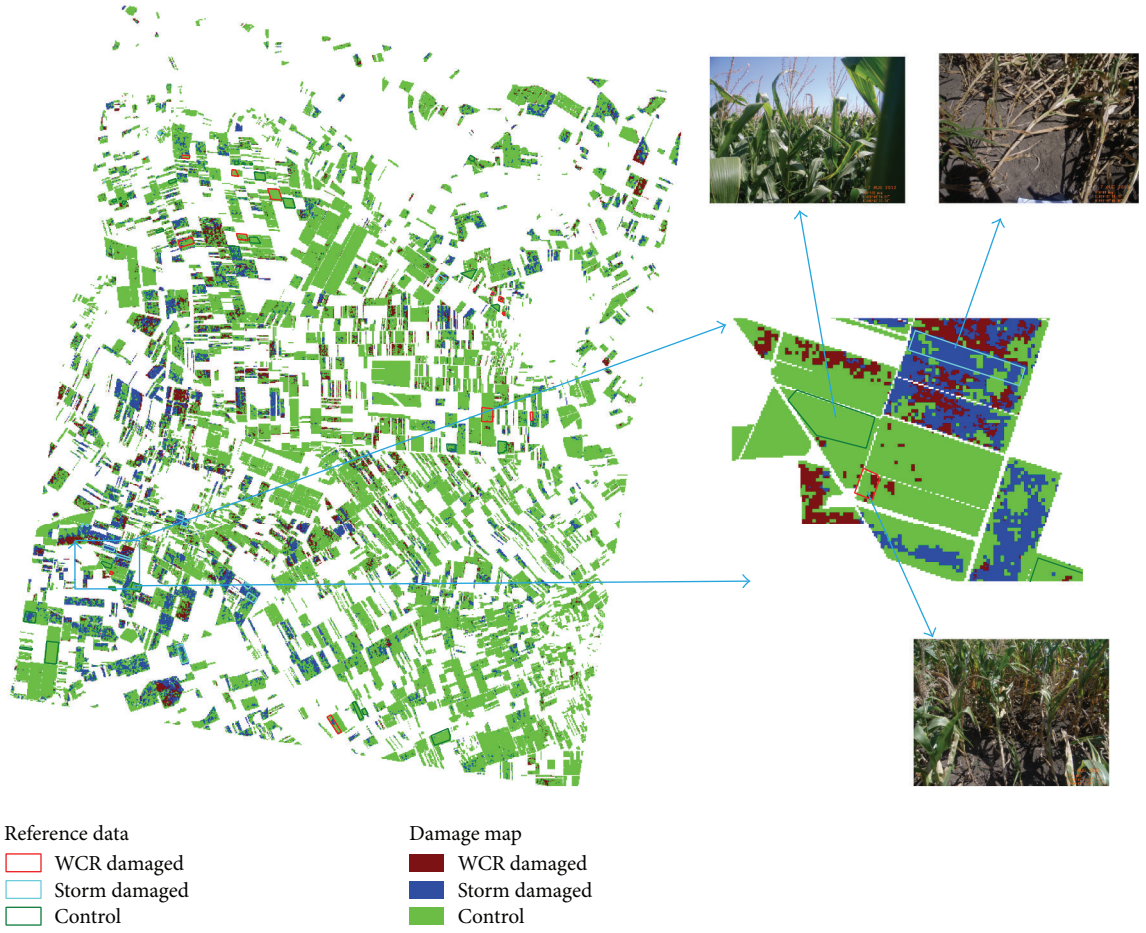

Figure 39: Damage map of maize parcels derived from integrated evaluation of radar and optical images.

polarimetric descriptors; it is difficult to find the most suitable one for the situation. An additional considerable output is that temporal development of changes both spectrally and geometrically differs. Therefore, better result requires usage of time series of radar and optical images as well.

Conflict of Interests

The authors declare that there is no conflict of interests regarding the publication of this paper.

Acknowledgments

Satellite image acquisition was carried out within the frame of our accepted SOAR-EU (called by ESA) proposal (EU-6741) entitled "Identification of structural changes in agriculture by radar polarimetry." The study was sponsored by Research, Technology and Innovation Foundation of Hungarian Development Agency in the frame of URKUT_10-1-2011-0038 project entitled "Methodology development for synergistic usage of optical and radar satellite images focusing on agricultural damages."

References

[1] J. W. Cable, J. M. Kovacs, X. Jiao, and J. Shang, "Agricultural monitoring in Northeastern Ontario, Canada, using multitemporal polarimetric RADARSAT-2 Data," *Remote Sensing*, vol. 6, no. 3, pp. 2343–2371, 2014.

[2] H. McNairn, J. J. van der Sanden, R. J. Brown, and J. Ellis, "The potential of RADARSAT-2 for crop mapping and assessing crop condition," in *Proceedings of the 2nd International Conference on Geospatial Information in Agriculture and Forestry*, Lake Buena Vista, Fla, USA, January 2000.

[3] C. Titin-Schnaider, "ONERA-Palaiseau (2000): radar polarimetry for vegetation observation," in *Proceedings of the CEOS SAR Workshop*, ESA SP-450, Toulouse, France, October 1999.

[4] P. Ferrazzoli, L. Guerriero, and G. Schiavon, "Experimental and model investigation on radar classification capability," *IEEE Transactions on Geoscience and Remote Sensing*, vol. 37, no. 2, pp. 960–968, 1999.

[5] S. R. Cloude and E. Pottier, "An entropy based classification scheme for land applications of polarimetric SAR," *IEEE Transactions on Geoscience and Remote Sensing*, vol. 35, no. 1, pp. 68–78, 1997.

[6] J. M. Lopez-Sanchez, F. Vicente, J. D. Ballester-Berman, and S. R. Cloude, "Polarimetric response of rice fields at C-band: analysis and applications," in *Proceedings of the 6th International*

Workshop on Science and Applications of SAR Polarimetry and Polarimetric Interferometry (POLinSAR '13), vol. SP-71, ESA, Frascati, Italy, January-February 2013.

[7] Z. Qi, A. G. Yeh, X. Li, and Z. Lin, "Land use and land cover classification using RADARSAT-2 polarimetric SAR image," in *Proceedings of the 7th ISPRS TC Symposium—100 Years ISPRS*, W. Wagner and B. Székely, Eds., vol. 38, part 7A, IAPRS, Vienna, Austria, July 2010.

[8] G. Nádor, G. Surek, D. Fényes et al., "Identification of structural changes caused by weed infection in agriculture by optical and radar data," in *Proceedings of the 5th ESA-ESRIN*, Frascati, Italy, January 2011.

[9] G. Surek, G. Nádor, D. Fényes, and L. Vasas, "Monitoring of western corn rootworm damage in maize fields by using integrated radar (ALOS PALSAR) and optical (IRS LISS, AWiFS) satellite data," *Geocarto International*, vol. 28, no. 1, pp. 63–79, 2013.

[10] G. Surek, G. Nádor, D. Á. Gera, I. Hubik, R. K. Anikó, and C. Török, "Identification of geometrical structural changes in agriculture by optical and radar data, poster presentation," in *Proceedings of the 6th International Workshop on Science and Applications of SAR Polarimetry and Polarimetric Interferometry (POLinSAR '13)*, Frascati, Italy, January-February 2013.

[11] C. López-Martínez, L. Ferro-Famil, and E. Pottier, PolSARpro v4.0 Polarimetry Tutorial, 2005, http://earth.eo.esa.int/polsarpro/tutorial.html.

[12] J.-S. Lee and E. Pottier, *Polarimetric Radar Imaging from Basics to Applications*, CRC Press, Taylor & Francis Group, 2009.

[13] P. Réfrégier and J. Morio, "Shannon entropy of partially polarized and partially coherent light with Gaussian fluctuations," *Journal of the Optical Society of America A: Optics and Image Science, and Vision*, vol. 23, no. 12, pp. 3036–3044, 2006.

[14] Y. W. Goodman, "Coherence of optical waves," in *Statistical Optics*, pp. 157–236, Wiley, 1985.

[15] Y. Yamaguchi, J. Nakamura, K. Aoyama, and H. Yamada, "Coherent decomposition of fully polarimetric radar data," in *Proceedings of the IEEE International Geoscience and Remote Sensing Symposium (IGARSS 2008)*, vol. 4, pp. 161–164, IEEE, Boston, Mass, USA, July 2008.

[16] Y. Yamaguchi, A. Sato, W.-M. Boerner, R. Sato, and H. Yamada, "Four-component scattering power decomposition with rotation of coherency matrix," *IEEE Transactions on Geoscience and Remote Sensing*, vol. 49, no. 6, pp. 2251–2258, 2011.

[17] Y. Yamaguchi, Y. Yajima, and H. Yamada, "A four-component decomposition of POLSAR images based on the coherency matrix," *IEEE Geoscience and Remote Sensing Letters*, vol. 3, no. 3, pp. 292–296, 2006.

[18] B. L. Welch, "The generalization of 'Student's' problem when several different population variances are involved," *Biometrika*, vol. 34, no. 1-2, pp. 28–35, 1947.

[19] R. G. Congalton and R. G. Oderwald, "Assessing landsat classification accuracy using discrete multivariate analysis statistical techniques," *Photogrammetric Engineering and Remote Sensing*, vol. 49, no. 12, pp. 1671–1678, 1983.

[20] G. H. Rosenfield and K. Fitzpatrick-Lins, "A coefficient of agreement as a measure of thematic classification accuracy," *Photogrammetric Engineering & Remote Sensing*, vol. 52, no. 2, pp. 223–227, 1986.